



# EUROPEAN SOUTHERN OBSERVATORY

Organisation Européenne pour des Recherches Astronomiques dans l'Hémisphère Austral  
Europäische Organisation für astronomische Forschung in der südlichen Hemisphäre

ESO - European Southern Observatory  
Karl-Schwarzschild Str. 2, D-85748 Garching bei München

---

## Very Large Telescope Paranal Science Operations VISIR User Manual

**Doc. No. VLT-MAN-ESO-14300-3514**

**Issue 90, Date 17/08/2012**

Y. Momany & the VISIR IOT

Prepared .....

Date Signature

C. Dumas

Approved .....

Date Signature

A. Kaufer

Released .....

Date Signature

This page was intentionally left blank

### Change Record

| Issue/Rev.  | Date       | Section/Parag. affected            | Reason/Initiation/Documents/Remarks   |
|---|------------|------------------------------------|---|
| 1.0   | 04/09/04   | creation                           | First release for science verification in P74 and OT proposals in P75.  |
| 1.1   | 10/12/04   | 2.4, 3.2, 6.2, 6.3, 7, 8           | update for P75 Phase2   |
| v76.1   | 01/02/05   | all                                | update for P76 CfP  |
| v76.2   | 06/07/05   | all                                | update for P76 Phase 2  |
| v76.3   | 14/07/05   | 4.8.1                              | Corrected Legend Fig 17   |
| v76.4   | 14/07/05   | Cover pages                        | Corrected typos   |
| v77.1   | 04/09/05   | 3.5,3.6,3.7,4.1,4.3,4.8.1,7,8.1,10 | update for P77 CfP  |
| v77.2   | 05/09/05   | 4.6                                | match imager overhead of CfP  |
| v77.3   | 20/12/05   | 1,2,3,4,3.6,4.2-4.4,4.7,7,8        | update for P77 Phase2   |
| v78.1   | 27/02/06   | 3.6, 3.10                          | update for P78 CfP  |
| v78   | 19/06/06   | cover, 2.2, 3.2, 4.3.1             | P78 release   |
| v79   | 30/11/06   | 4.8                                | P79 release   |
| v80   | 28/02/07   | 3.1, 4.2.1, 5.1, 6.2, 8.2          | P80 release, burst mode included  |
| v81   | 31/08/07   | 3.1, 4.2.1, 4.3.2                  | P81 release, new filters included   |
| v87   | 22/09/10   | 4.3.2, 8.2, 8.3                    | P87 release, <b>Exclusion</b> of <i>K</i> -band in science imaging templates  |
|   |            | 3.2.5                              | P87 release, update of HR allowed $\lambda_c$   |
|   |            | 8.2                                | First line of Table.7 modified  |
|   |            |                                    | P87 release, non-availability of <i>jitter</i> with <i>IMG – GenericChopNod</i>   |
| v88   | 22/02/2011 | 4.1                                | P88 release, upper limit of 5 filters in a single service mode OB   |
|   |            | 4.4                                | P88 release, UCAC3 substituting USNO for guide stars selections.  |
| v89   | 31/08/2011 | all                                | P89 release, removing most references to the old DRS detector, and reporting the first properties of the AQUARIUS detector. |
| v90   | 26/02/2012 | 1                                  | Update the new schedule of the VISIR upgrade.   |
| v90   | 17/08/2012 | all                                | New updates after the Commissioning#1.  |
| v1.0, v1.1, v76.1: edited by R. Siebenmorgen, E. Pantin, M. Sterzik<br>v76.2–4, v77.1-3, updated by A. Smette.<br>v78 – 80, updated by L. Vanzi.<br>v87 – 90, updated by Y. Momany. |            |                                    |   |

# Contents

|          |   |           |
|----------|---|-----------|
| <b>1</b> | <b>VISIR Upgrade Project</b>                              | <b>1</b>  |
| 1.1      | Detector Upgrade . . . . .                                | 1         |
| 1.2      | Low Resolution Spectroscopy . . . . .                     | 1         |
| 1.3      | Precipitable Water Vapor . . . . .                        | 1         |
| <b>2</b> | <b>Introduction</b>                                       | <b>3</b>  |
| <b>3</b> | <b>Observing in the MIR from the ground</b>               | <b>3</b>  |
| 3.1      | The Earth's atmosphere . . . . .                          | 3         |
| 3.2      | The spatial resolution . . . . .                          | 3         |
| 3.3      | MIR background . . . . .                                  | 4         |
| 3.4      | Chopping and nodding . . . . .                            | 4         |
| 3.5      | Sensitivity . . . . .                                     | 7         |
| <b>4</b> | <b>Instrument description and offered observing modes</b> | <b>8</b>  |
| 4.1      | Imager . . . . .  | 8         |
| 4.2      | Spectrometer . . . . .                                    | 11        |
| 4.2.1    | Slit widths . . . . .                                     | 11        |
| 4.2.2    | Resolution . . . . .                                      | 12        |
| 4.2.3    | Low resolution: offered central wavelengths . . . . .     | 12        |
| 4.2.4    | Medium resolution: offered central wavelengths . . . . .  | 12        |
| 4.2.5    | High resolution: offered central wavelengths . . . . .    | 12        |
| 4.3      | Calibration units . . . . .                               | 13        |
| 4.4      | Detectors . . . . .                                       | 13        |
| 4.4.1    | Detector Architecture . . . . .                           | 15        |
| 4.4.2    | Detector Readout . . . . .                                | 15        |
| 4.4.3    | Detector Thermal Oscillations . . . . .                   | 16        |
| 4.4.4    | Detector Dark Current . . . . .                           | 16        |
| 4.4.5    | Detector Linearity . . . . .                              | 16        |
| 4.5      | Data acquisition system . . . . .                         | 19        |
| <b>5</b> | <b>Observing with VISIR at the VLT</b>                    | <b>20</b> |
| 5.1      | Proposal preparation . . . . .                            | 20        |
| 5.2      | Telescope observing parameters . . . . .                  | 21        |
| 5.2.1    | Instrument orientation on the sky . . . . .               | 21        |
| 5.2.2    | Chopping parameters . . . . .                             | 22        |
| 5.2.3    | Nodding parameters . . . . .                              | 23        |
| 5.3      | Target acquisition . . . . .                              | 23        |
| 5.3.1    | Introduction . . . . .                                    | 23        |
| 5.3.2    | Description . . . . .                                     | 24        |

|           |   |           |
|-----------|---|-----------|
| 5.4       | Guide stars . . . . .   | 26        |
| 5.5       | Brightness limitations . . . . .  | 27        |
| 5.6       | Overheads . . . . .   | 27        |
| 5.7       | Calibration observations . . . . .  | 28        |
| 5.8       | OBs Classification . . . . .  | 29        |
| 5.9       | Known problems . . . . .  | 30        |
| <b>6</b>  | <b>VISIR data</b>   | <b>30</b> |
| 6.1       | Data format . . . . .   | 30        |
| 6.2       | Pipeline . . . . .  | 30        |
| 6.3       | VISIR spectrometer data . . . . .   | 31        |
| <b>7</b>  | <b>VISIR templates description</b>  | <b>32</b> |
| 7.1       | Acquisition . . . . .   | 32        |
| 7.2       | Observing with the imager . . . . .                                       | 32        |
| 7.3       | Observing with the spectrometer . . . . .                                 | 34        |
| 7.4       | Calibration . . . . .   | 35        |
| <b>8</b>  | <b>Checklist</b>  | <b>36</b> |
| 8.1       | Phase 1 . . . . .   | 36        |
| 8.2       | Phase 2 . . . . .   | 36        |
| <b>9</b>  | <b>Appendix: VISIR template parameters</b>                                | <b>38</b> |
| 9.1       | Observation . . . . .   | 40        |
| 9.2       | Calibration . . . . .   | 42        |
| <b>10</b> | <b>Appendix: Filter transmission curves</b>                               | <b>44</b> |
| <b>11</b> | <b>Appendix: Observed sensitivities in various spectroscopic settings</b> | <b>47</b> |

## List of acronyms

|       |  |
|-------|--|
| BIB   | Blocked impurity band                            |
| BLIP  | Background limited performance                   |
| BOB   | Broker of observation blocks                     |
| DIT   | Detector integration time                        |
| ETC   | Exposure time calculator                         |
| FWHM  | Full width at half maximum                       |
| ICS   | Instrument control software                      |
| IR    | Infrared   |
| IRACE | Infrared array control electronics               |
| MIR   | Mid infrared                                     |
| OB    | Observing block                                  |
| P2PP  | Phase 2 proposal preparation                     |
| PAE   | Preliminary acceptance in Europe                 |
| pfov  | pixel field of view                              |
| PSF   | Point spread function                            |
| S/N   | Signal-to-noise ratio                            |
| UT    | Unit telescope                                   |
| VISIR | VLT imager and spectrometer for the mid infrared |
| TCS   | Telescope control system                         |
| TMA   | Three mirrors anastigmatic                       |
| WCU   | Warm calibration unit                            |

# 1 VISIR Upgrade Project

During the period May-October 2012 (P89) VISIR will go through the implementation of its upgrade project. It is expected that VISIR will be offered back to regular service and visitor mode observations from November 2012 onwards.

The post-upgrade VISIR performance is expected to be significantly better. However, no details can be provided at the moment. For the time being, we here list the major modifications that VISIR P90 science users will need to plan their proposals. The astronomical community is encouraged to monitor the latest news on the upgrade, reported on:

<http://www.eso.org/sci/facilities/paranal/instruments/visir/upgradeproject.html>.

## 1.1 Detector Upgrade

The major part of the upgrade project concerns the replacement of the current detector (DRS 256 × 256 pixel array) with The Raytheon AQUARIUS 1024 × 1024 pixel array. This hardware upgrade is expected to significantly improve the VISIR performance in terms of field coverage and sensitivity. The new AQUARIUS detector will be offered in two pixel scales: 0'045 and 0'076, SF and IF respectively. The projected and usable field of view is 40'0 × 40'0 and 62'0 × 62'0 arcseconds.

As for Exposure time calculation, the astronomical community is invited to use the well-established DRS detector sensitivities (both for spectroscopy and imaging) as provided in Tables, 2, 3, 6 and 7. Indeed, the new AQUARIUS detector has proven to show better performance, however a final characterization of the achieved sensitivities is to await the commissioning and science verification. The cosmetic quality of the AQUARIUS detector is proven to be excellent. The regions of masked pixels and stripes (c.f. Fig. 12) are not present anymore.

## 1.2 Low Resolution Spectroscopy

The second major improvement is that concerning the N-band 8 – 13 $\mu$ m Low Resolution Spectroscopy. This was achieved by means of a grism, and had the disadvantage of requiring 4 independent exposures in order to cover the 8 – 13.5 $\mu$ m range. The introduction of the low resolution prism ( $R \simeq 300$  for a 0'3 slit) will allow to achieve the same wavelength coverage in a single exposure and reach improved sensitivities.

## 1.3 Precipitable Water Vapor

The amount of Precipitable Water Vapor (PWV) present in the Earth's atmosphere can heavily impact on Mid-infrared observations. However, the effect of PWV is strongly dependent on wavelength. Whereas a PWV column of 3 mm or larger is generally acceptable for observations in the N-band, the sensitivity of observations in the Q-band depends strongly on the PWV contents, and typically can be done under PWV columns between 1 and 3 millimeters. Operations-wise, a prior knowledge of the PWV content will seriously impact on efficient service and visitor mode VISIR observations. As part of the VISIR upgrade project, and starting December 2011, real-time PWV monitor is now available on Paranal<sup>1</sup>.

The commissioning of the PWV monitor shows that it meets all specifications:

---

<sup>1</sup>[http://www.eso.org/tecarch/Documents/VLT/14300-mid\\_ir\\_imager\\_spectrometer/14330-VISIR\\_Upgrade/SoW\\_for%20\\_RS\\_campaign\\_5504.pdf](http://www.eso.org/tecarch/Documents/VLT/14300-mid_ir_imager_spectrometer/14330-VISIR_Upgrade/SoW_for%20_RS_campaign_5504.pdf)

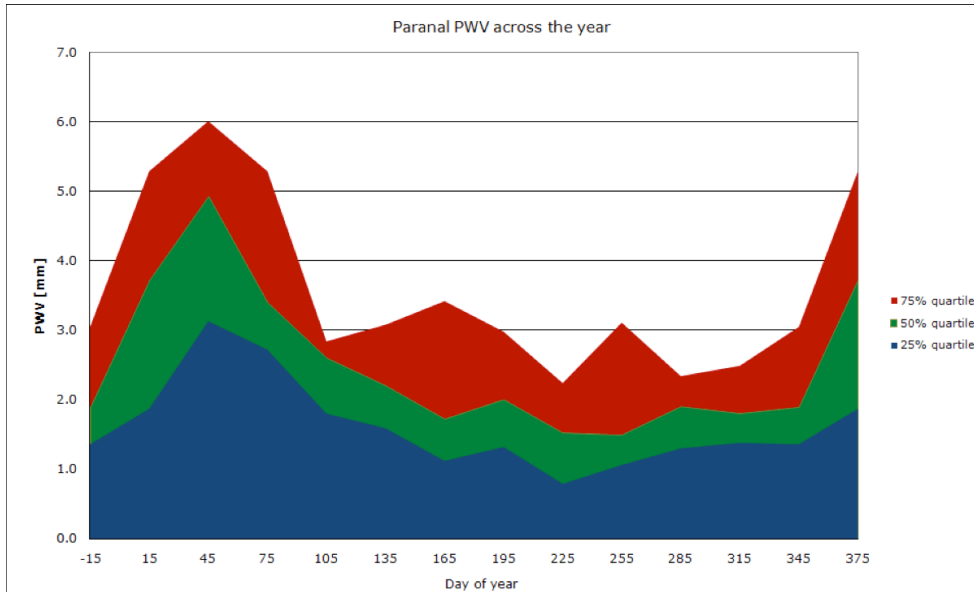


Figure 1: Average PWV distribution over Paranal across the year.

- PWV range 0.5-9 mm validated
- PWV precision: ca 30  $\mu\text{m}$
- PWV accuracy: ca 0.1 mm
- High time resolution (sec)
- All sky pointing, 2D capability
- Autonomous operation

The median PWV over Paranal is 2.1 mm, with strong seasonal variations (see Fig. 1). The fraction of time in which the PWV contents over Paranal is lower than 1 mm is about 10%. The PWV value will be used as user-defined constraint parameter starting Period 90 (October 2012- April 2013).



## 2 Introduction

The VLT spectrometer and imager for the mid-infrared (VISIR), built by CEA/DAPNIA/SAP and NFRA/ASTRON, provides diffraction-limited imaging at high sensitivity in two mid-infrared (MIR) atmospheric windows: the N-band between  $\approx 8$  to  $13 \mu\text{m}$  and the Q-band between  $16.5$  and  $24.5 \mu\text{m}$ . In addition, it offers a slit spectrometer with a range of spectral resolutions between 150 and 30000.

The MIR provides invaluable information about the warm dust and gas phase of the Universe. Micron sized particles such as silicates, silicon carbide, carbon, coals, aluminum oxides or polycyclic aromatic hydrocarbon (PAH) molecules are major contributors to the thermal MIR emission. The gaseous phase emits through a large number of ionic and atomic lines. Examples are NeII ( $12.8 \mu\text{m}$ ) and the pure rotation lines of molecular hydrogen at  $8.02$ ,  $9.66$ ,  $12.27$  and  $17.03 \mu\text{m}$ .

Because of the very high background from the ambient atmosphere and telescope, the sensitivity of ground-based MIR instruments cannot compete with that of space-born ones. However, ground based instruments mounted on large telescopes offer superior spatial resolution. For example VISIR at the VLT provides diffraction limited images at  $\sim 0.3''$  (FWHM) in the N band. This is an order of magnitude better than what can be reached by the Spitzer Space Telescope (SST).

The VISIR user manual is structured as follows: Basic observing techniques of ground-based MIR instruments are summarized in §3. §4 provides a technical description of VISIR and its offered observing modes offered. An overview on how to observe with VISIR at the VLT can be found in § 5. A description of the structure of the imaging and spectroscopic data files is given in § 6. A checklist to help the preparation of OBs is available in § 8. Acquisition, observing and calibration templates are explained in § 7.

We strongly recommend to consult:

<http://www.eso.org/instruments/visir/> for additional information and updates. For support during proposal preparation and OB submission, please contact ESO's User Support Department ([usd-help@eso.org](mailto:usd-help@eso.org)).

## 3 Observing in the MIR from the ground

### 3.1 The Earth's atmosphere

Our atmosphere absorbs the majority of the MIR radiation from astronomical sources. The main absorbing molecules are  $\text{H}_2\text{O}$ ,  $\text{CH}_4$ ,  $\text{CO}_2$ ,  $\text{CO}$ ,  $\text{O}_2$ ,  $\text{O}_3$ . However, the atmosphere is quite transparent in two atmospheric windows: the N and Q bands. They are centered around  $10$  and  $20 \mu\text{m}$ , respectively. The transmission in the N band is fairly good at a dry site and becomes particularly transparent in the wavelength range  $10.5$ - $12 \mu\text{m}$ . However, the transmission of the Q band is rapidly decreasing with wavelength and can be viewed as the superposition of many sub-bands having a typical spectral coverage of  $\Delta\lambda = 1 \mu\text{m}$  ( $\text{PWV} \leq 3\text{mm}$ ) at an average transmission of 60%. Observations in this band require low water vapor content in the atmosphere. The atmospheric transmission in the N and Q bands is displayed in Fig. 2.

### 3.2 The spatial resolution

The spatial resolution of an instrument is ultimately limited either by the diffraction of the telescope or the atmospheric seeing. The diffraction limit as measured by the diameter of the first Airy ring

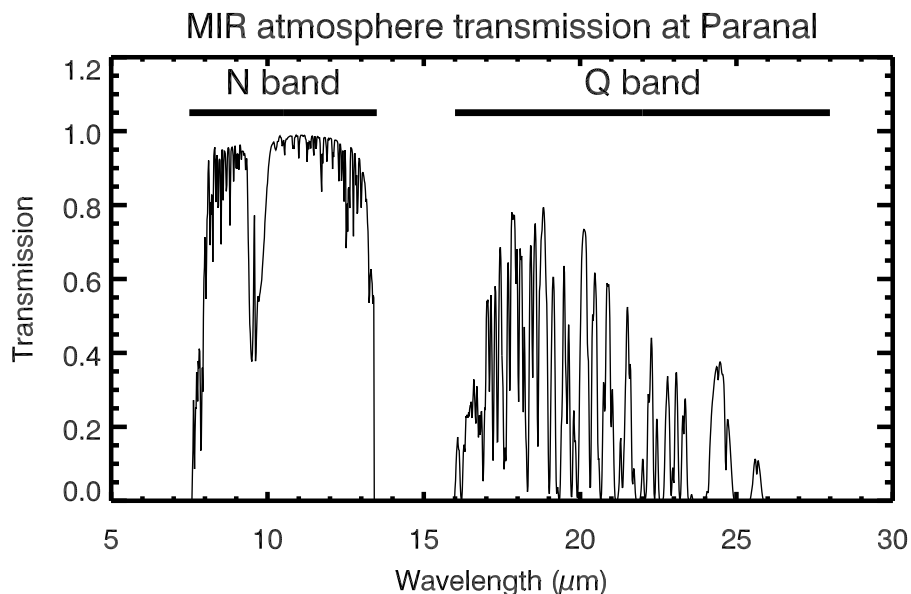


Figure 2: MIR atmospheric transmission at Paranal computed with HITRAN for an altitude of 2600 m and 1.5 mm of precipitable water vapor at zenith. The US standard model atmosphere is used.

increases with wavelength as  $1.22 \lambda/D$ , where  $\lambda$  is the observing wavelength and  $D$  the diameter of the telescope mirror (see solid line in Fig. 3). The wavelength dependence of the seeing can be derived by studying the spatial coherence radius of the atmosphere in the telescope beam and is to first order approximated by the Roddier formula, where the seeing is  $\propto \lambda^{-0.2}$  (see dot-dashed lines in Fig. 3). However, initial results from VISIR data indicate that this formula overestimates the measured MIR seeing at Paranal by 20–50%, as the size of a UT mirror is comparable to the turbulence outer scale. As a result, VISIR data are already diffraction limited for optical seeing below  $0.6''$ . The results of measures obtained in 2005 are shown in Fig. 4.

### 3.3 MIR background

The atmosphere does not only absorb MIR photons coming from astrophysical targets, but also emits a strong background with the spectral shape of a black-body at about 253 K (Kirchhoff's law). The telescope gives an additional MIR background. The VLT telescopes emit at 283 K with a preliminary emissivity estimate of  $< 15\%$  in N. The VISIR instrument is cooled to avoid internal background contamination. The detectors are at  $\sim 5 - 6$  K and the interior of the cryostat at 33 K. The background radiation at  $10\mu\text{m}$  is typically  $m_N = -5 \text{ mag/arcsec}^2$  ( $3700 \text{ Jy/arcsec}^2$ ) and at  $20\mu\text{m}$   $m_Q = -7.3 \text{ mag/arcsec}^2$  ( $8300 \text{ Jy/arcsec}^2$ ).

Consequently, the number of photons reaching the detector is huge, often more than  $10^8$  photons/s. Therefore, the exposure time of an individual integration - the Detector Integration Time (DIT) - is short, of the order of a few tens of milli-seconds in imaging mode.

### 3.4 Chopping and nodding

The basic idea to suppress the MIR background is to perform differential observations, using the chopping/nodding technique.

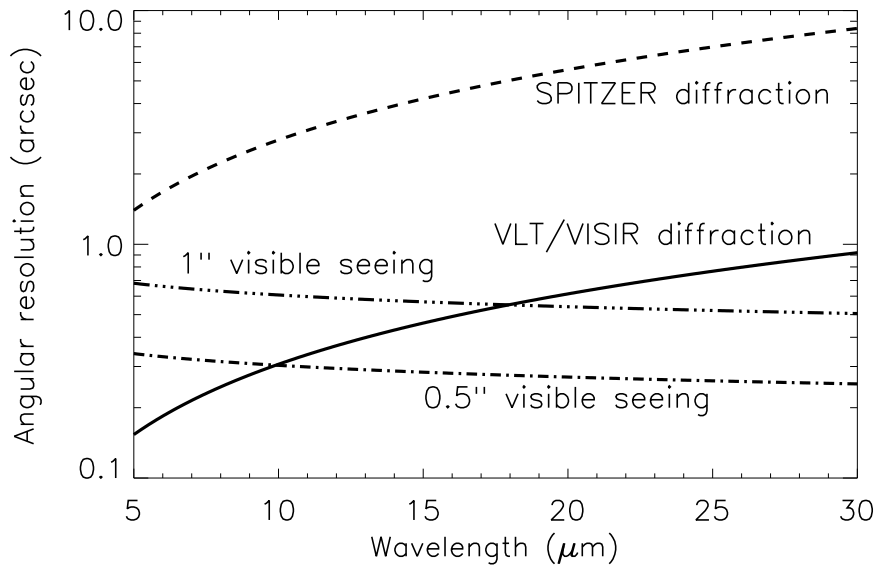


Figure 3: VLT diffraction limit (full line) versus seeing. The Spitzer Space Telescope diffraction limits (dashed) are shown for comparison. The Roddier dependence is shown for two optical seeing (dashed-dot).

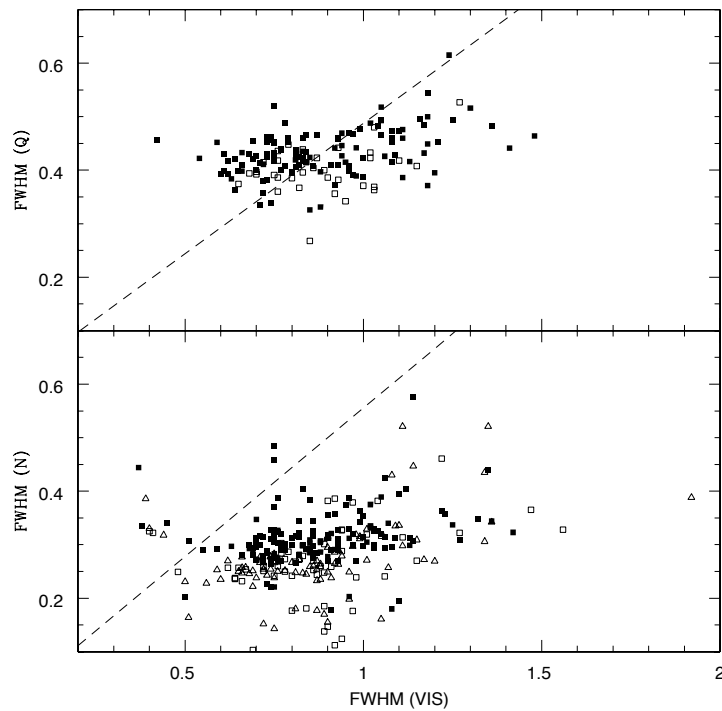


Figure 4: Measures of the VISIR image quality versus optical seeing obtained during 2005. The dashed lines indicates the prediction of Roddier's formula.

In the chopping technique two observations are performed. One set of exposures on–source, include the background and the astronomical source. A second set of off–source exposures measures the pure background. The on– and off–source observations have to be alternated at a rate faster than the rate of the background fluctuations. In practice, it is achieved by moving the secondary mirror of the telescope. For VISIR at Paranal, a chopping frequency of 0.25 Hz has been found to be adequate for N–band imaging observations, while 0.5 Hz are adopted for Q–band imaging. Spectroscopic observations are performed with lower chopper frequencies, at 0.1 Hz or less.

The chopping technique cancels most of the background. However, the optical path is not exactly the same in both chopper positions. Therefore a residual background remains. It is varying at a time–scale which is long compared to that of the sky. This residual is suppressed by nodding, where the telescope itself is moved off–source and the same chopping observations as in the on–source position is repeated.

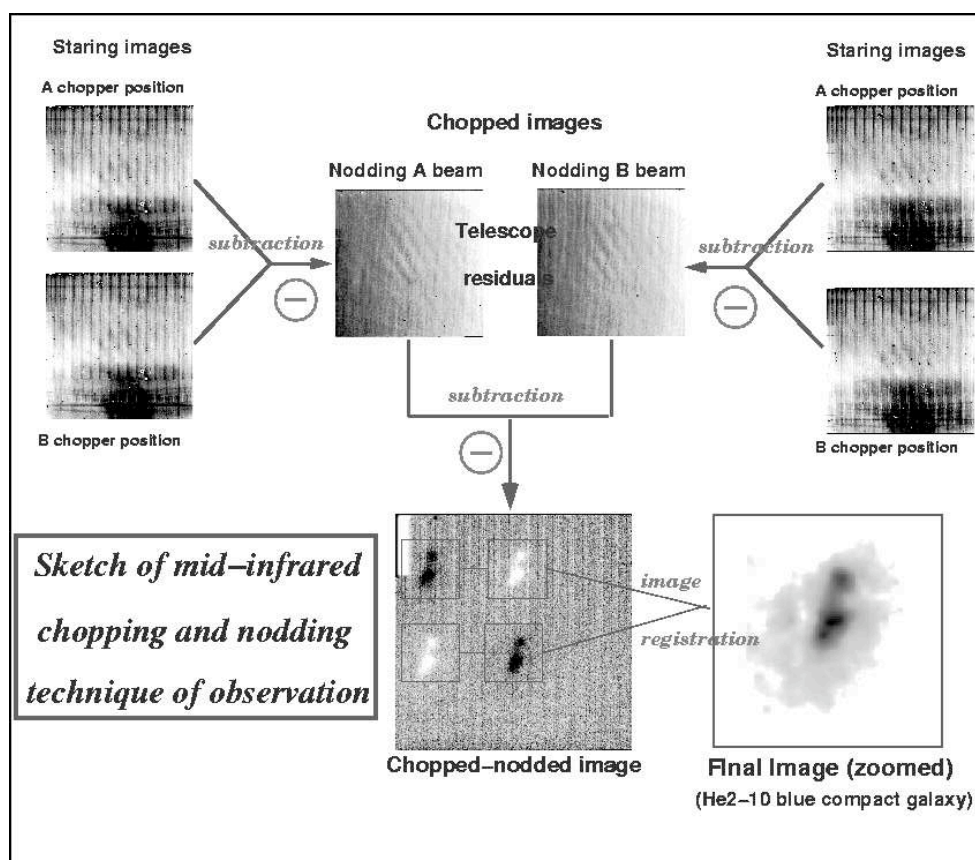


Figure 5: Illustration of the chopping and nodding technique on observations of the blue compact galaxy He2-10. The galaxy only appears after chopping and nodding (courtesy VISIR commissioning team, June 2004).

An illustration of the chopping and nodding technique is shown on Fig. 5. Depending on the choice of chopping and nodding amplitudes and directions, up to 4 images of the source can be seen on the frame and used for scientific analysis. Of course, the *free* field–of–view on the chop/nod images can be severely reduced depending on the particular chopping and nodding parameters chosen.

### 3.5 Sensitivity

Measurements of VISIR sensitivities are based on observations of mid-infrared calibration standard stars (Cohen et al. 1999, AJ 117, 1864). In imaging mode, the stars are recorded in the small field (0.045'') and intermediate field (0.076'') by perpendicular chopping and nodding patterns with amplitudes of 10''. Calibrators are frequently observed during the night (§5.7). Flux and noise levels are extracted by multi-aperture photometry using the curve-of-growth method: the aperture used for all 4 beams in a given frame is the one for which the flux to noise ratio is the largest. By combining all 4 beams, *the sensitivity in a given set-up (filter, field of view) is defined as the limiting flux of a point-source detected with a S/N of 10 in one hour of on-source integration.*

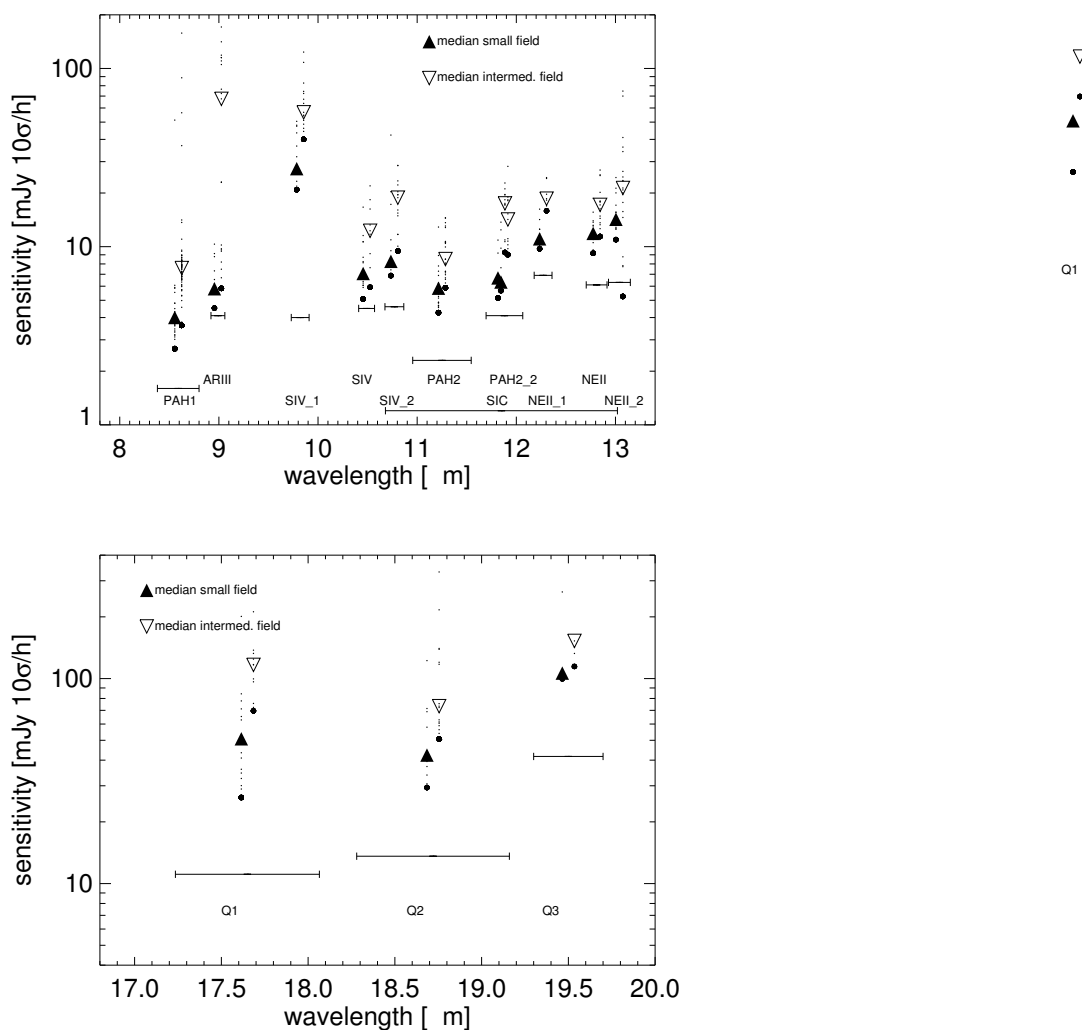


Figure 6: **Measured on the old DRS detector but also valid for Period 90.** Sensitivities for the VISIR imager for the N (top) and Q-band (bottom). Small and intermediate field observations are displaced for clarity. Background noise limits are indicated for the individual filter bandpasses.

The growing calibration database allows a statistical analysis of the sensitivity with respect to instrumental and atmospheric conditions. The values for each filter given in Table 2 refer to the median of more than 600 different observations during Sept.-Dec. 2004. A graphical compilation is presented in Fig. 6 for the N and Q-band imaging filters. Some of the best measurements approach theoretical expectations, i.e. they are close to background limited performance (BLIP).

Sensitivity estimates for the VISIR spectroscopy observing modes are obtained in a similar way. However, in this case, chopping and nodding are executed in parallel. Consequently, only 3 beams are obtained, with the central one containing twice as much flux as the two other ones.

Table 5 to 6 list typical sensitivities measured in low, medium and high resolution modes away from strong sky emission lines for the wavelength ranges offered in P76. Figures 20 to 36 in the Appendix (§ 11) shows the dependence of sensitivity on wavelength.

The median sensitivities are the reference for classification of VISIR service mode observations, and the basis to assess the feasibility of an observing program. In particular, *classification* of service mode OBs will be based on sensitivity measurements made at zenith. Calibrations will be provided following the guidelines given in § 5.7. For up to date information, please consult <http://www.eso.org/instruments/visir>. The use the VISIR exposure time calculator (ETC, located at <http://www.eso.org/observing/etc/>) is recommended to estimate the on-source integration time.

## 4 Instrument description and offered observing modes

VISIR offers two spatial scales in imaging and several spectral resolution modes in slit spectroscopy. The imager and spectrograph are two sub-instruments. They have independent light paths, optics and detectors. The cryogenic optical bench is enclosed in a vacuum vessel. The vessel is a cylinder, 1.2 m long and 1.5 m in diameter. Standard Gifford-McMahon closed-cycle coolers are used to maintain the required temperature: 33 K for most of the structure and optics and < 15 K for the parts near the detector. The detectors are cooled down to ~ 5 – 6 K.

### 4.1 Imager

The imager is based on an all-reflective design. The optical design is shown in Fig. 7. It consists of two parts:

- A collimator, which provides an 18 mm diameter cold stop pupil in parallel light: As generally designed for IR instruments, the pupil of the telescope is imaged on a cold stop mask to avoid stray-light and excessive background emission. The collimator mirror (M1) is a concave aspherical mirror. It is followed by a folding flat mirror (M2) which eases the mechanical implementation.
- A set of three objectives mounted on a wheel. Each objective is based on a three mirror anastigmatic (TMA) system. Each of the TMA's is made of three conic mirrors.

The 0.045'' (small field, SF) and 0.076'' (intermediated field, IF) pixel scale are offered (Table 1). These offered pixel fields of view (pfov) ensure a proper sampling of the images in the N and Q-band.

| Pixel size | Field of view |
|------------|---------------|
| 0'076      | 62'0 × 62'0   |
| 0'045      | 40'0 × 40'0   |

Table 1: The offered pixel scales of the IMAGER detector, and the corresponding **usable** field of view. The pixel size of the AQUARIUS 1k×1k detector is 30 μm .

The filter wheel is located just behind the cold stop pupil mask. The list of filters offered is given in Table 2. The transmission curves of the filters measured at 35 K are plotted in the Appendix. Starting Period 81 and in addition to the ones listed in Table 2, another set of filters is offered. Their characteristics are summarized in Table 3.

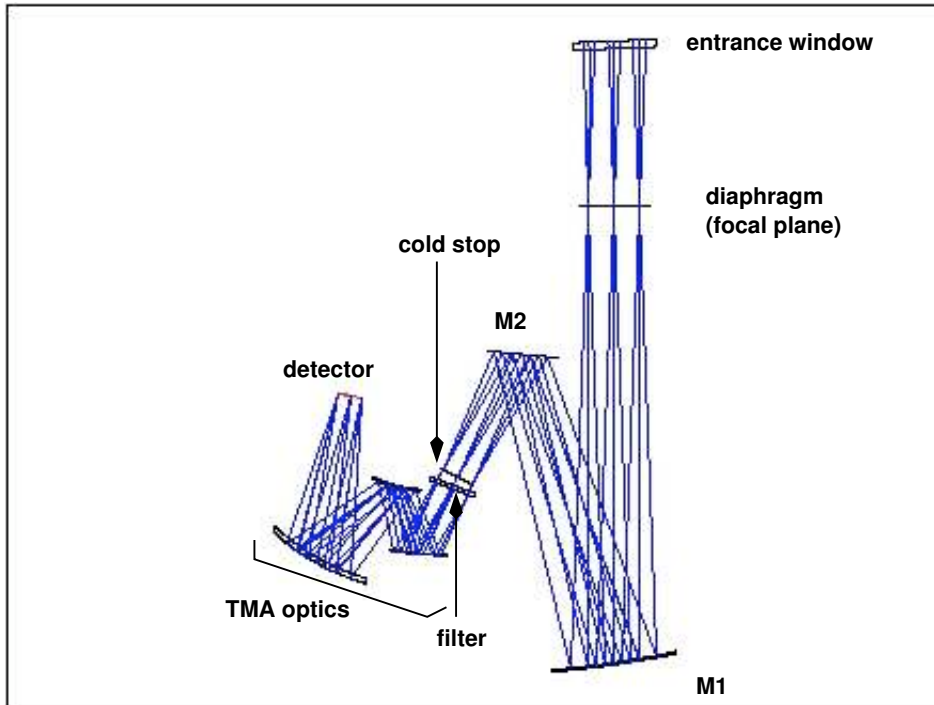


Figure 7: The optical path of the imager in the intermediate field ( $0'.076$ ) is shown from the entrance window down to the detector.

The burst read out is offered for the imager in visitor mode only. The burst read out allows the user to save every single DIT (Detector Integration Time) frame of the exposure. In this way it is possible to follow rapidly evolving events or to improve the spatial resolution by taking short enough exposures to freeze the atmospheric turbulence. This mode can be used only for objects bright enough to provide a S/N high enough in a single elementary exposure. Typical flux limits are of the order of 5 Jy in N and 10 Jy in Q. Some compromise between sensitivity and time resolution can be reached by averaging a number of elementary frames. Further and more up-to-date information can be found at: <http://www.eso.org/instruments/visir/inst/> .

| filter | $\lambda_c$<br>( $\mu\text{m}$ ) | half-band width<br>( $\mu\text{m}$ ) | maximum<br>transmission<br>(%) | sensitivity<br>(mJy $10\sigma/1\text{h}$ ) |                   |     |
|--------|----------------------------------|--------------------------------------|--------------------------------|--|-------------------|-----|
|        |                                  |                                      |                                | theory<br>(BLIP)                           | median<br>SF   IF |     |
| PAH1   | 8.59                             | 0.42                                 | 77                             | 1.6  | 5                 | 8   |
| ArIII  | 8.99                             | 0.14                                 | 72                             | 4.1  | 6                 | 70  |
| SIV_1  | 9.82 <sup>1</sup>                | 0.18                                 | 72                             | 4.0  | 30                | 60  |
| SIV    | 10.49                            | 0.16                                 | 70                             | 4.5  | 8                 | 13  |
| SIV_2  | 10.77 <sup>1</sup>               | 0.19                                 | 70                             | 4.6  | 9                 | 20  |
| PAH2   | 11.25                            | 0.59                                 | 75                             | 2.3  | 6                 | 9   |
| SiC    | 11.85                            | 2.34                                 | 75                             | 1.2  | 7                 | 18  |
| PAH2_2 | 11.88 <sup>1</sup>               | 0.37                                 | 58                             | 4.1  | 7                 | 15  |
| NeII_1 | 12.27 <sup>1</sup>               | 0.18                                 | 51                             | 6.9  | 12                | 20  |
| NeII   | 12.81                            | 0.21                                 | 64                             | 6.1  | 12                | 18  |
| NeII_2 | 13.04                            | 0.22                                 | 68                             | 6.3  | 15                | 22  |
| Q1     | 17.65                            | 0.83                                 | 59                             | 11.1                                       | 50                | 120 |
| Q2     | 18.72                            | 0.88                                 | 49                             | 13.6                                       | 50                | 80  |
| Q3     | 19.50                            | 0.40                                 | 50                             | 41.7                                       | 100               | 160 |

Table 2: **Sensitivity values are still valid for Period 90 proposal preparation.** VISIR imager filter characteristics, following the manufacturer specifications, except for the central wavelengths noted with <sup>1</sup> which were re-determined with a monochromator and the WCU because they deviate from specifications. The last 3 columns give, respectively, the theoretical expectations under BLIP and excellent weather conditions, and the measured median sensitivities for the Small and Intermediate Field obtained in various weather conditions. The measured sensitivities were obtained using the curve-of-growth method on data obtained in perpendicular chopping/nodding directions (4 beams).

| filter | $\lambda_c$<br>( $\mu\text{m}$ ) | half-band width<br>( $\mu\text{m}$ ) | sensitivity<br>(mJy $10\sigma/1\text{h}$ ) |    |
|--------|----------------------------------|--------------------------------------|--|----|
|        |                                  |                                      | SF   | IF |
| B 8.7  | 8.92                             | 0.97                                 | -  | -  |
| B 9.7  | 9.82                             | 0.84                                 | 9  | 20 |
| B 10.7 | 10.65                            | 1.37                                 | 5  | 8  |
| B 11.7 | 11.52                            | 0.85                                 | 5  | 6  |
| B 12.4 | 12.47                            | 0.99                                 | 8  | 12 |
| J 7.9  | 7.76                             | 0.55                                 | 14   | 25 |
| J 8.9  | 8.70                             | 0.73                                 | 3  | 5  |
| J 9.8  | 9.59                             | 0.94                                 | 7  | 10 |
| J 12.2 | 11.96                            | 0.52                                 | 8  | 10 |

Table 3: **Sensitivity values are still valid for Period 90 proposal preparation.** VISIR imager filter characteristics determined with a monochromator and the WCU. The last 2 columns give the measured median sensitivities for the Small and Intermediate Field obtained in good weather conditions. The measured sensitivities were obtained using the curve-of-growth method on data obtained in perpendicular chopping/nodding directions (4 beams).



## 4.2 Spectrometer

VISIR offers slit spectroscopy at three spectral resolutions with a pixel scale of  $0''.076$ . This is obtained by means of two arms, one with low order gratings for the low and medium spectral resolution, the other with large echelle gratings providing high spectral resolution.

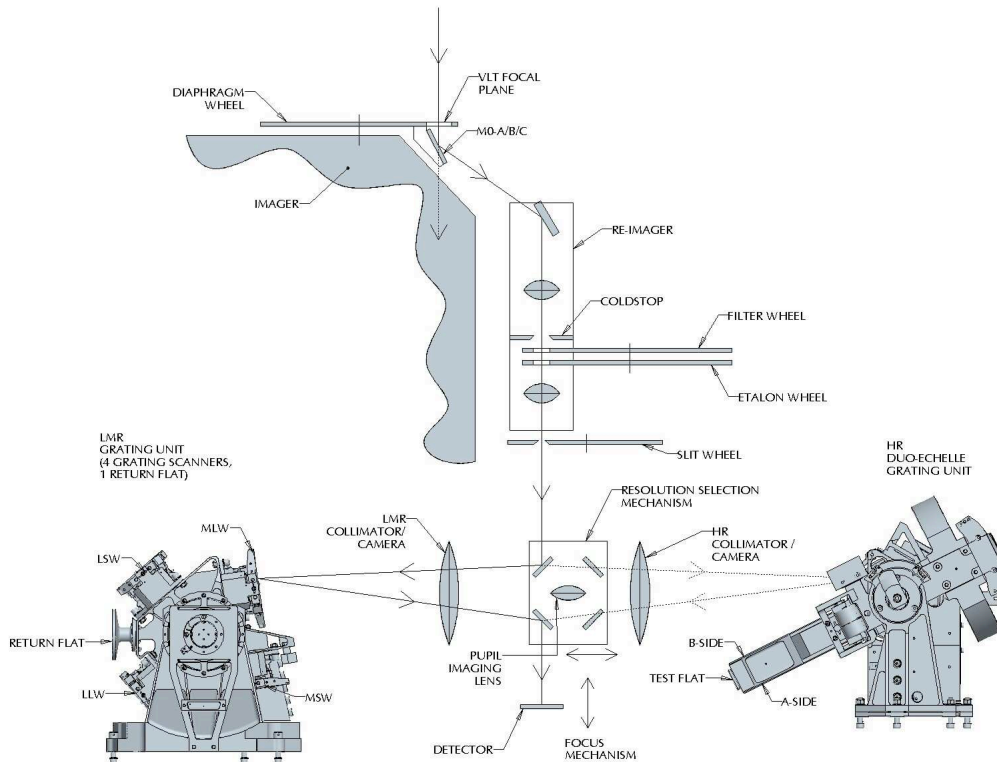


Figure 8: Schematic layout of the design of the VISIR spectrometer.

The long slits have a length of  $32.5''$ . The short slits, only used in high-resolution cross-dispersed mode, have a length of  $4.1''$ . The all-reflective optical design of the spectrometer uses two TMA systems in double pass (pass 1: collimator, pass 2: camera). A schematic layout of the VISIR spectrometer design is shown in Fig. 8. The 3-mirror system of the low- and medium-resolution arm gives a 53 mm (diameter) collimated beam; the collimated beam diameter in the high-resolution arm is 125 mm. Both subsystems image the spectrum onto the same detector; selection between the two spectrometer arms is done by two pairs of folding flat mirrors. In front of the actual spectrometer subsystems is a reflective re-imager consisting of two off-axis paraboloids and three folding flats. The re-imager provides a 16 mm diameter cold-stop pupil in parallel light and transforms the incoming VLT Cassegrain beam of  $F:13.4$  to an  $F:10$  beam at the spectrometer entrance. The spectrometer slit wheel is also equipped with a very wide slit ( $15.3''$ ) named OPEN in P2PP. It gives the possibility to make imaging with the spectrometer detector and is used for object acquisition and centering on the detector.

The list of available filters for spectroscopic acquisition offered is given in Table 4, together with their measured bandpasses and approximate sensitivities for image acquisition.

### 4.2.1 Slit widths

Three different slit widths ( $0.4''$ ,  $0.75''$  and  $1''$ ) are offered for all settings. For over-sized widths (e.g. for the  $1''$  slit with respect to the diffraction limit around  $10\mu\text{m}$ ) the spectral resolution of a

| filter | $\lambda_c$<br>( $\mu\text{m}$ ) | half-band width<br>( $\mu\text{m}$ ) | sensitivity<br>(mJy/10 $\sigma$ /1h) |
|--------|----------------------------------|--------------------------------------|--------------------------------------|
| N_SW   | 8.85                             | 1.35                                 | 40                                   |
| N_LW   | 12.1                             | 1.9                                  | 40                                   |
| ArIII  | 8.94                             | 0.11                                 | 200                                  |
| NeII_1 | 12.35                            | 0.50                                 | 80                                   |
| NeII_2 | 12.81                            | 0.10                                 | 50                                   |

Table 4: VISIR spectrometer filter characteristics. The filters transmissions have been determined with a monochromator and the WCU. The last column list the measured median sensitivities which were obtained using the curve-of-growth method on data obtained in parallel chopping/nodding directions (3 beams).

point-source spectrum is better than the one of the sky spectrum; in addition, the zero-point of the wavelength calibration will be affected by an incorrect centering of the object within the slit.

#### 4.2.2 Resolution

In the N band, the low-resolution and medium resolution modes provide spectral resolving power of  $\sim 300$  and  $\sim 3000$  (Table 5), respectively. In high resolution long-slit mode, narrow wavelength ranges around the 8.02 [H2\_S4], 12.813 [Ne II] and 17.03  $\mu\text{m}$  [H2\_S1] line are offered. With the 1'' slit the measured spectral resolution is  $R \sim 15000$  (Table 6), and a minimum flux in an emission line below  $10^{-16}$  W/m<sup>2</sup>/arcsec<sup>2</sup> can be achieved. This value corresponds to an approximate sensitivity limit around 1 Jy in the continuum. A high-resolution, cross-dispersed mode with a 4.1'' short slit is available for a number of wavelength settings (Table 6).

Please consult <http://www.eso.org/instruments/visir> for the latest update of the list of offered modes and slits.

#### 4.2.3 Low resolution: offered central wavelengths

Following the VISIR upgrade project, and throughout Period 90, the N-band 8 – 13  $\mu\text{m}$  Low Resolution Spectroscopy will require only one exposure to cover the 8 – 13  $\mu\text{m}$  range. This is achieved by replacing the current gratings with a new ( $R \simeq 300$  for a 0'.3 slit) prism. The sensitivities measured on the old DRS detector still apply for Period P90 proposal preparation. These are  $\sim 50$  mJy at 10 $\sigma$ /1h in the clean regions of the spectrum. Offered slits have widths of 0.40, 0.75 and 1.00''.

#### 4.2.4 Medium resolution: offered central wavelengths

In Medium Resolution mode, the central wavelength  $\lambda_c$  can be freely chosen within the wavelength ranges listed in Table 5. Note that the exposure time calculator (ETC) cannot currently provide estimates of S/N for  $\lambda < 7.6\mu\text{m}$ . Table 5 provides offered sensitivities.

#### 4.2.5 High resolution: offered central wavelengths

The VISIR spectrometer offers a high-resolution long-slit mode for 3 passbands centered in the wavelengths of the [H2\_S4], [NeII] and [H2\_S1] lines. A wider range of wavelengths is accessible

| $\lambda_c$ – range<br>( $\mu\text{m}$ ) | $\Delta\lambda$<br>( $\mu\text{m}$ ) | grating<br>order | spect.–resol.<br>(measured, 1''slit) | dispersion<br>(pixels/ $\mu\text{m}$ ) | sensitivity<br>(mJy at $10\sigma$ in 1h) |
|--|--------------------------------------|------------------|--------------------------------------|--|--|
| 7.5 – 8.0                                | 0.195                                | 2                | $\sim 3500$                          | $\sim 2192$                            | 1000                                     |
| 8.0 – 9.3                                | 0.188                                | 2                | $\sim 3500$                          | $\sim 2267$                            | 200                                      |
| 10.2 – 13.0                              | $\sim 0.21$                          | 2                | $\sim 3500$                          | $\sim 2417 - 1733$                     | 200                                      |
| 17.1 – 19.0                              | 0.37                                 | 1                | $\sim 1800$                          | $\sim 1158$                            | 1200                                     |
| 20.12                                    | 0.36                                 | 1                | $\sim 1800$                          | 720                                    | 1200                                     |

Table 5: VISIR medium resolution settings. The first column gives the minimum and maximum allowed values for the central wavelength ( $\lambda_c$ ) in the given setting. The wavelength range per setting is given in the 2nd column ( $\Delta\lambda$ ). The spectral resolution, measured with a 1''slit, is given in the 3rd column. **The dispersion is given in the 4th column, and has been estimated for the new AQUARIUS detector pixel size.** Typical offered sensitivities are given in the last column. Examples of dependence of sensitivity with wavelength are shown in Figures 21 to 24. Offered slits have widths of 0.40, 0.75 and 1.00''.

with the high-resolution cross-dispersed mode, with a 4.1'' long slit.

Offered modes and sensitivities are given in Table 6. The ETC offers the possibility to take into account the earth motion to predict the observed wavelength of a given line depending on the foreseen date and time of observations. In particular, this feature allows to determine the dates when the emission line under study would appear at the same wavelength as a sky line.

### 4.3 Calibration units

A warm calibration unit (WCU) is located on top of the VISIR vacuum enclosure. The WCU is also called star simulator. It simulates either a monochromatic point source with adjustable wavelength or an extended black-body source with adjustable temperature. A selection mirror allows to switch from the telescope to the simulator beam. It can be used for calibration and tests, also during daytime. Fig. 9 shows the unit on top of the enclosure.

### 4.4 Detectors

The VISIR imager and spectrometer are currently equipped with two new AQUARIUS  $1k \times 1k$  detectors, with pixel size of  $30 \mu\text{m}^2$ . In principle, this provide a field of view that is  $\sim 5 - 6$  times larger than that offered by the old DRS  $256 \times 256$  detector. However, following the commissioning of the detector upgrade, the unvignetted and usable part of the AQUARIUS detector is smaller than the entire detector (890 pixels in the Y-axis). Availing the two pixel scales of  $0'.045$  and  $0'.076$  the finally offered field of view are  $40'.0 \times 40'.0$  and  $62'.0 \times 62'.0$ , respectively.

The AQUARIUS array was developed at Raytheon Vision Systems at Santa Barbara USA. The development was funded by ESO to upgrade the VISIR instrument at VLT, for next generation VLTI instruments, and for the future mid-IR candidate instrument (METIS) at the E-ELT. For a detailed presentation of the AQUARIUS detector we refer the reader to Ives et al. (Proc. SPIE 8453-38), in the following we will highlight on the major properties of the detector.

To properly operate in the mid-IR window, the AQUARIUS detector is designed to deliver low thermal background, high quantum efficiency, and high sensitivity. With respect to conventional ones, these goals have been achieved by the introduction of a new class of photo-conductors, called the Impurity Band Conduction (IBC, Raytheon designation). Their Si:As IBC design achieved higher

| mode | $\lambda_c$<br>( $\mu\text{m}$ ) | $\Delta\lambda$<br>( $\mu\text{m}$ ) | line           | order | R     | dispersion<br>(pixels/ $\mu\text{m}$ ) | sensitivity<br>Jy $10\sigma/1\text{h}$ |
|------|----------------------------------|--------------------------------------|----------------|-------|-------|--|--|
| HR   | 7.800 – 8.100                    | 0.02420                              | [H2_S4]        | 17B   | 32000 | 17573                                  | ~3                                     |
| HR   | 12.738 – 12.882                  | 0.03571                              | [Ne II]        | 11A   | 17000 | 11908                                  | ~0.9                                   |
| HR   | 16.800 – 17.200                  | 0.05156                              | [H2_S1]        | 8B    | 14000 | 8250                                   | <10                                    |
| HRX  | 8.970 – 9.140                    | 0.02270                              | [ArIII]        | 16A   | 27100 | 18757                                  | ~ 4                                    |
| HRX  | 9.360 – 9.690                    | 0.02325                              | [H2_S3]        | 15A   | 25000 | 18290                                  | ~5                                     |
| HRX  | 10.480 – 10.540                  | 0.03160                              | [SIV],[CoII]   | 12B   | 24000 | 13407                                  | ~4                                     |
| HRX  | 11.540 – 11.570                  | 0.03210                              | HD (0,0) R(10) | 12B   | 23400 | 13333                                  | ~ 2                                    |
| HRX  | 11.762                           | 0.03260                              | [CIIV]         | 12A   | 19100 | 13067                                  | ~ 3                                    |
| HRX  | 12.210 – 12.760                  | 0.03864                              | [H2_S2]        | 11B   | 20000 | 11007                                  | ~1.5                                   |
| HRX  | 12.814 – 13.364                  | 0.03550                              | [NeII]         | 11A   | 17500 | 11917                                  | ~2                                     |
| HRX  | 16.390                           | 0.03551                              | [CoIII]        | 9A    | 17300 | 12100                                  | ~ 12                                   |
| HRX  | 16.925                           | 0.05240                              | [CoI]          | 8B    | 14100 | 8067                                   | ~ 8                                    |
| HRX  | 17.790 – 17.980                  | 0.04707                              | [PIII],[FeII]  | 8A    | 13140 | 9000                                   | ~ 4                                    |
| HRX  | 18.246                           | 0.04182                              | [NiII]         | 8A    | 14600 | 10133                                  | ~ 8                                    |
| HRX  | 18.680 – 18.960                  | 0.06569                              | [SIII]         | 7B    | 11150 | 6450                                   | ~ 4                                    |
| HRX  | 21.295                           | 0.04196                              | [NaIV]         | 7A    | 14300 | 10097                                  | ~ 9                                    |

Table 6: VISIR high resolution long-slit (HR) and cross-dispersed (HRX) modes. The second column gives the minimum and maximum allowed values for the central wavelength ( $\lambda_c$ ) in the given setting. The wavelength range per setting is given in the 3rd column ( $\Delta\lambda$ ).  $R$  is the theoretical spectral resolution. Offered slits have widths of 0.40, 0.75 and 1.00". Note that the range 12.210 – 12.760 also covers HD (0,0) R(9), while the [NeII] emission line can be observed up to  $z \approx 0.038$ . **The dispersion is given in the 7th column, and has been estimated for the new AQUARIUS detector pixel size.**

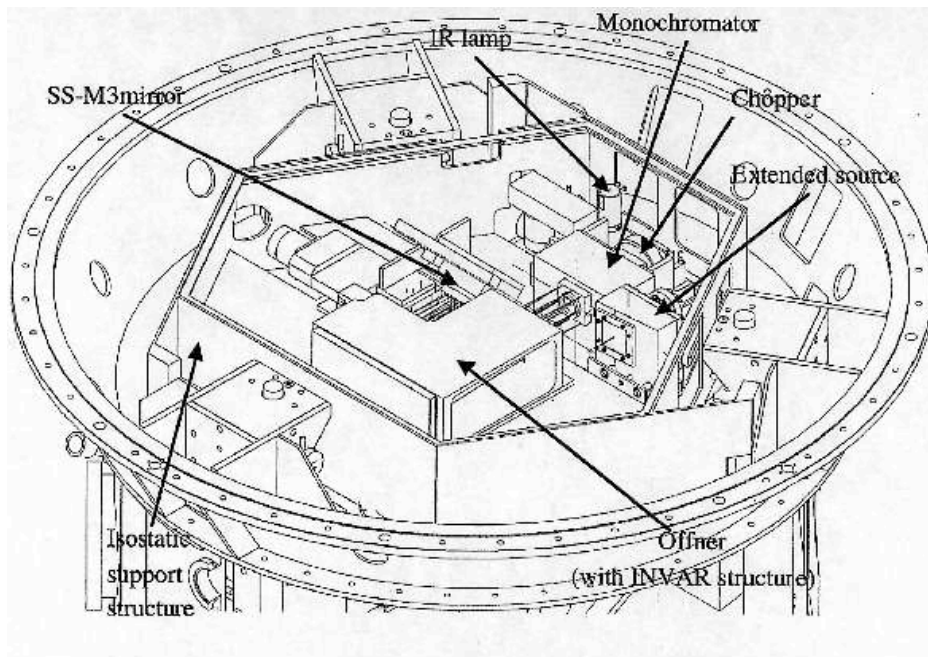


Figure 9: Schematic drawing of the warm calibration unit on top of the VISIR vessel.

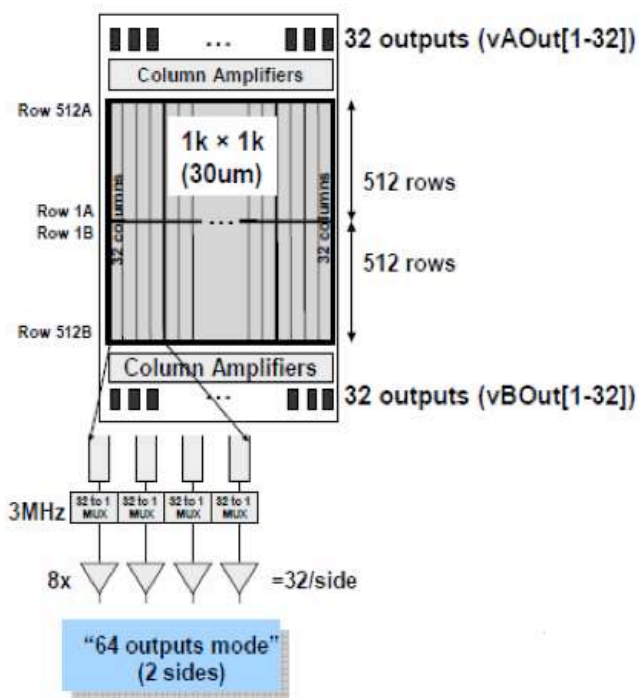


Figure 10: Left panel shows the AQUARIUS multiplexing readout scheme. Right panel shows the detector mounted in its socket.

sensitivities by decreasing the thickness of the photo-conductor and increasing the doping of the Si:As diodes.

#### 4.4.1 Detector Architecture

Figure 10 displays the architecture of the AQUARIUS detector. It is split into two perpendicular areas; each made of 512 rows and 1024 columns. Each area has 32 outputs, such that, each output is configured to read out 32 x 512 pixels, all 64 outputs from the two areas being read in parallel. This readout scheme also allows for 16 outputs rather than 64 to simplify system design for low background applications. With this multiplexer configuration it is possible to read the detector out at 150 Hz (7 milli-seconds) frame rates, each output operational at 3 MHz pixel rates.

#### 4.4.2 Detector Readout

A windowed readout is also possible. VISIR users can select a number of rows can be read (from the center outwards) with the remaining rows reset automatically. For example, a 1024 x 150 sized window, centered in the middle of the device, can be readout at 1 kHz (0.001 milli-seconds) frame rates. There is no advantage to windowing in the column direction since all outputs run in parallel. All the typical detector read out modes are available and user-programmable with the simple control of five external clock control lines. These readout modes include:

- Global Reset: where all pixels are reset at the same time;
- Rolling mode, where a row is read then immediately reset, then the next row is read and reset and so forth, for a programmable row time which can overlap the read of the next row;

- Non-Destructive Read without reset; and
- Row Reset Level Read (RRLR) where a row can be reset then read.

Correlated Double Sampling, Fowler Sampling and Up-The-Ramp Sampling can all be implemented using any combination of these different read out modes. The multiplexer also has test rows, top and bottom and each output row of 32 pixels also has an on-chip generated reference level which can be read out and used for low frequency noise suppression.

At the time this user manual is released, the readout mode has not been decided yet. This will be done during the second commissioning of VISIR at the end of October 2012, and further details of the properties of the readout will be provided.

#### 4.4.3 Detector Thermal Oscillations

Mid-IR detectors suffer some thermal oscillations that occur at a frequency of 1 Hz. This is due to the fact that the Closed Cycle Coolers used to cool the detector and optical part *do not* provide a constant temperature in their cooling cycle. These thermal oscillations can result in additional detector noise, estimated to be 250 DN which translates to an additional noise of approximately 50  $e^-$  rms added in quadrature to the read noise. The solution to this problem was to mount a large block of lead, approximately 0.6 kg in weight. This smoothed the thermal oscillation by a factor of at least fifty.

#### 4.4.4 Detector Dark Current

Mid-IR detectors operate at a temperature range that is set by the Closed Cycle Coolers; typically 6 – 9 K. Lower operating temperatures allow to minimize the leakage and, most importantly, the dark current. Laboratory experiments showed that the dark current ranged between  $\sim 2200$  and  $0.56$   $e^-/pixel/s$  at 10.0 and 5.6 K, respectively. The upgrade operational goals aimed at reaching a  $\sim 1.0$   $e^-/pixel/s$  and this was achieved at an operating temperature of 7 K.

#### 4.4.5 Detector Linearity

The AQUARIUS detector linearity was derived for both the high gain and the low gain configurations. The left panel of Fig.11 displays the measured signal level as a function of exposure time. Typically this data is taken in a non-destructive read mode such that many hundreds of frames are taken between the signal detector starvation level up to its saturation level. A linear fit was applied to the data points between 15,000 – 40,000 DN, and the differences between the fit and the data points is plotted for the high gain setup (right panel of Fig.11). Over this signal range the detector shows an excellent linearity of the order of  $\pm 0.5\%$ . For this particular detector, the gain and therefore the detector saturation level and read noise can be changed by a factor of approximately eight.

At the operating temperature of the detector ( $\sim 6-7$  K), the dark current, which is the signal obtained when the detector receives no photons, is negligible compared to the background generated by the photons emitted by the telescope and the atmosphere. The dark current is removed by the observation technique (chopping or nodding).

The detectors have a switchable pixel (“well”) capacity. The large capacity is used for broad-band imaging and the small capacity for narrow band imaging and spectroscopy. Detector saturation due to the enormous MIR background is avoided by a storage capacity of  $0.6 \cdot 10^6$   $e^-$  in small and  $6.0 \cdot 10^6$



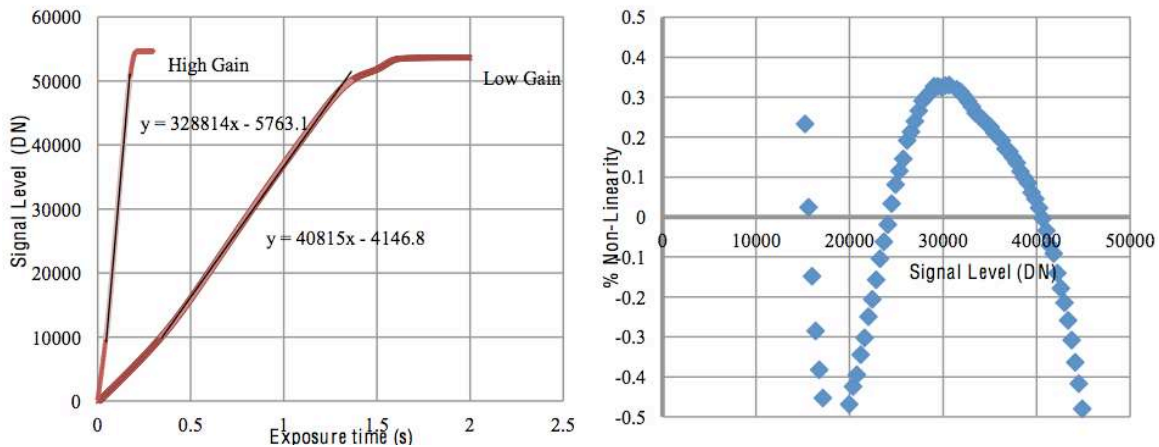


Figure 11: Left panel displays the measured AQUARIUS detector linearity for both high and low gain read modes. Right panel displays the non-linearity as a function of the signal level, as computed for the high gain setup.

$e^-$  in large capacity modes, respectively. The detector integration time (DIT) is a few milli-seconds in broad-band imaging and may increase to  $\sim 2$  s in high resolution spectroscopy.

The DIT is determined by the instrument software using a user-selectable algorithm. The options are:

1. **AUTO:** in this case the sky background value is estimated by examining the background level in exposures obtained with the lowest available DIT. Consequently, the DIT value is increased until the background level is conservatively within the linearity operating regime of the detector, and the highest *good* DIT is selected.
2. **GOOD-WEATHER:** in this case one assumes that weather conditions (in terms of PWV and transparency) are nominally good and selects a single tabulated DIT value (typically of the order of 8 milli-seconds) that will ensure the operation of the detector at a reasonable 25% of the potential well.
3. **BRIGHT-SOURCE:** this option is useful in case the science target is a significantly bright source, and one is interested in selecting the lowest possible DIT value to ensure the non-saturation of the detector.

The new AQUARIUS detector cosmetic testing shows that it does not show the high fraction of bad pixels seen in the old DRS detector. Moreover, the AQUARIUS detector can be considered free from stripping effects and ghosts. Moreover, due to the new spectroscopic/imaging detectors readout structure (from the center outwards) it is now recommended that the scientific/standard stars targets are not placed in the very center of the detectors, but slightly offset by few arcseconds, either above or below the central division of the detectors.

For period 90, it is advised to observe only sources fainter than 500 Jy in N and 2500 Jy in Q. Due to the low flux levels, eventual detector artifacts are less important in spectroscopy. As in previous periods however, it is advised that a `TEL.CHOP.THROW` between 9 to 13'' should be avoided, until a full characterization of the AQUARIUS detector is done.

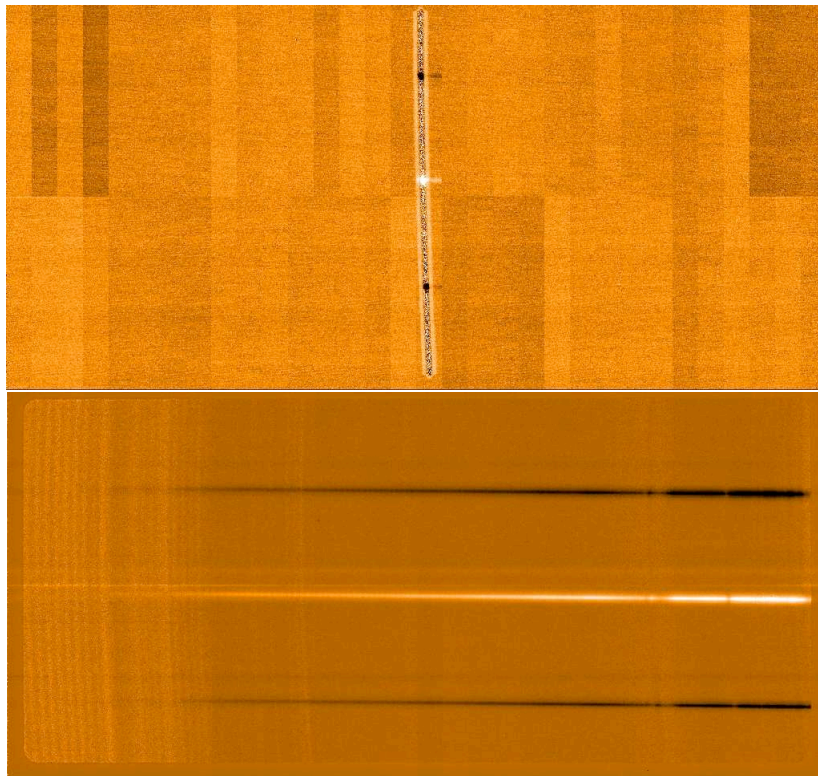


Figure 12: Upper: An example of the good cosmetics on the new Aquarius detector, used for acquisition of a Cohen standard in the  $1''.0$  slit. Note the central division of the detector due to the intrinsic central-outward readout, and how the target was placed slightly above. Lower: A sequence of chop/nod, reduced spectra obtained in the Low Resolution mode, covering the entire N-band with a single exposure. The TEL.CHOP.THROW was set to  $10''$ .



## 4.5 Data acquisition system

As part of the upgrade project, the VISIR new AQUARIUS detectors will be controlled by the new NGC acquisition system. In imaging the read–out rate of the detector is high. Up to 200 frames per second are read for a minimum detector integration time of  $DIT = 5$  ms. Such a frame rate is too high to store all exposures. One VISIR image is of size  $1024 \times 1024$ ; each pixel is coded with 4 bytes (long integer). Thus one read–out has a size of 262 kB.

The current version of the NGC (by default) provides output files in the format of “fits-extensions”. These are structured in the following way: (i) a general long header, (ii) a number of sub images (HALF-CYCLE), which have their own short headers, and these are the intermediate results in a given nodding position; and lastly (iii) a single INTERMEDIATE-result-image for that given nodding position. During each chopping cycle the elementary exposures are added in real time and stored into disk. In particular, at a chopping frequency of  $f_{\text{chop}} = 0.25$  Hz, every  $T_{\text{chop}} = 4$  s, two VISIR HALF-CYCLE images are stored as frames in the fits-extension file.

The number of chopping cycles, within one nodding position, is defined by the time spent integrating in that nodding position,  $T_{\text{nod}}$ . This nodding period is typically  $T_{\text{nod}} = 90$  s for science observations. The chopper frequency, DIT and also  $T_{\text{nod}}$  are predefined by the system. The number of saved A–B frames in one FITS file is:

$$N_{\text{cycl\_chop}} = T_{\text{nod}}/T_{\text{chop}} \quad (1)$$

The number of nodding cycles is computed from the total integration time as given by the observer. The total number of stacked images for each secondary position, respectively chopper half cycle, is  $NDIT$ . This parameter is computed according to:

$$NDIT = (2 \cdot DIT \cdot f_{\text{chop}})^{-1} - NDITSKIP \quad (2)$$

and is given by the system. It depends on DIT, chopping frequency and  $NDITSKIP$ : some read–outs at the beginning of each chopper half cycle are rejected during stabilization of the secondary. Typical stabilization times of the secondary are 25 ms. The number of rejected exposures is given by  $NDITSKIP$ . Similar, during stabilization after each telescope movement, respectively nodding position, a number  $NCYSKIP$  of chopping cycles is ignored. The timing organization of data is shown in Fig. 13.

The total on source integration time is:

$$t_{\text{source}} = 4 \cdot N_{\text{cycl\_nod}} \cdot N_{\text{cycl\_chop}} \cdot NDIT \cdot DIT \quad (3)$$

The total rejected time is:

$$t_{\text{skip}} = 4 \cdot N_{\text{cycl\_nod}} \cdot DIT \cdot (NDITSKIP \cdot N_{\text{cycl\_chop}} + NDIT \cdot NCYSKIP) \quad (4)$$

and the total observing time is:

$$t_{\text{tot}} = t_{\text{source}} + t_{\text{skip}} \quad (5)$$

Typical duty cycles ( $t_{\text{source}}/t_{\text{tot}}$ ) are about 70%.

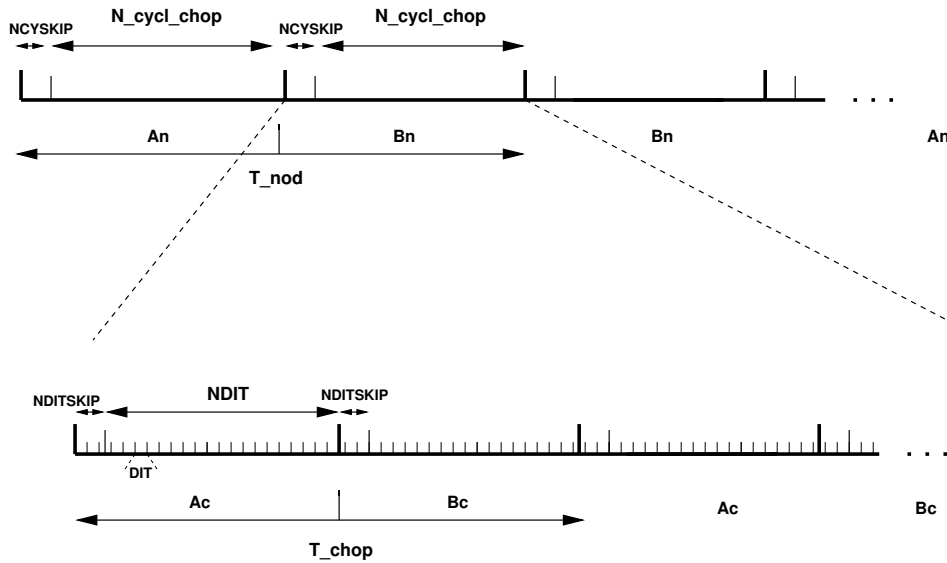


Figure 13: Data timing in VISIR.  $A_c$  and  $B_c$  refer to the two chopper positions,  $A_n$  and  $B_n$  refer to the two nodding (telescope) positions. Note the  $A_n B_n B_n A_n$  cycle sequence for the nodding to save observing time.

## 5 Observing with VISIR at the VLT

### 5.1 Proposal preparation

Tools are available to prepare the observations, either during phase 1 (call for proposals), or during phase 2 (creation of observing blocks by the observer):

- The *exposure time calculator* (ETC available at <http://www.eso.org/observing/etc/>) may be used to estimate the integration time needed to obtain the required S/N for a given instrument setting; because of the numerous sky absorption lines, (see Fig. 20 and following), it is recommended to display the S/N as a function of wavelength when using the spectrograph ETC. This advice is particularly relevant for spectroscopic settings with wavelengths centered at  $8.8\mu\text{m}$  as they will be strongly affected by the detector feature at this wavelength.
- As for all VLT instruments, astronomers with granted VISIR telescope time prepare their observations using *the phase 2 proposal preparation tool* (P2PP), described at <http://www.eso.org/sci/observing/phase2/P2PPTool.html>. Acquisitions, observations and calibrations are coded via observing templates. One or more templates build up an observing block (OB). They contain all the information necessary for the execution of a complete observing sequence. An overview of the available VISIR templates and their parameters is given in §7 of this manual.
- For each science template, the user has to provide a finding chart so that the target can be acquired. In addition to the general instruction on how to create these finding charts, see <http://www.eso.org/sci/observing/phase2/SMGuidelines.html>, the following VISIR requirements apply:
  - All finding charts have to be made using existing infrared (K-band or longer wavelength) images. Typically, 2MASS or DENIS K-band images are acceptable, although higher spatial resolution may be preferable.

- If the wavelength at which the finding chart has been taken is different from that of the science observation, e.g. a K-band finding chart for a  $10\mu\text{m}$  spectroscopic template, the user has to describe clearly how to identify the target at the observing wavelength in the README section of the program description. Adequate examples of such comments are:

- \* The target will be the brightest source in the field of view at  $10\mu\text{m}$ .
- \* At  $10\mu\text{m}$ , there will be two bright sources in our field of view. The science target is the southernmost of these two.

- It is mandatory to check that a guide star brighter than  $V=13$  within a field of  $7.5$  arcmin radius around the science target is available. This can be done using the guidecam tool (see <http://www.eso.org/instruments/visir/doc>). See § 5.4

Note that observations close to zenith during meridian crossing should be avoided, because of fast tracking speeds that do not allow proper background cancelation after nodding.

A final recommendation concerning service mode observations is that no more than 5 filters are grouped together in a single Observing Blocks. This is rather necessary for a proper calibration of each single filter. Moreover, it is also recommended that N and Q band filters are not grouped together as the Q-band sensitivities can be quite lower from that in the N-band.

Questions related to the VISIR Phase 1 and Phase 2 observing preparation should be directed to the User Support Department ([usd-help@eso.org](mailto:usd-help@eso.org)).

## 5.2 Telescope observing parameters

### 5.2.1 Instrument orientation on the sky

By default, the imager orientation is such that North is at the top and East is to the left. For the spectrometer, the detector is flipped in the North direction, so that the North is to the bottom and the East is to the left, with the slit orientation along the South-North direction. Figure 14 summarizes the situation.

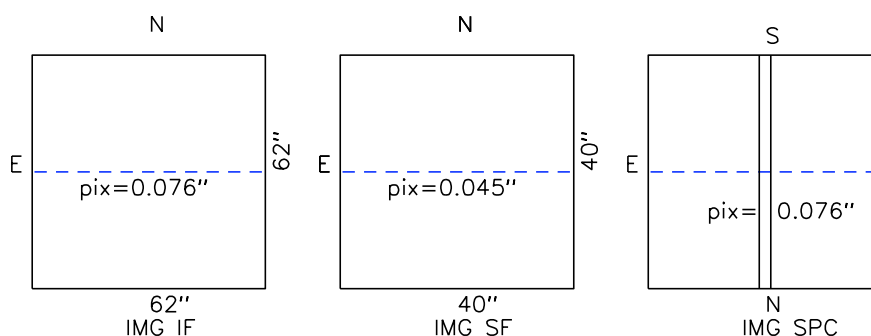


Figure 14: Field orientation and scale for the imaging and spectroscopic modes of VISIR. The blue dashed line highlight the center of the detectors, marking the central-outward readout.

Since VISIR is mounted on a rotator at the Cassegrain focus of Melipal, it is possible to change the default orientation of VISIR on the sky, for example, to obtain the spectra of two objects, A and B, at once. The parameter `TEL.ROT.OFFANGLE`, defaulted to  $0^\circ$ , is used for this purpose. If  $PA$  represents

the required position angle of object B relative to A, measured on the sky east of north (i.e., counted positively from north to east) within the range 0 to 360°, then setting

$$\text{TEL.ROT.OFFANGLE} = 360 - \text{PA}$$

allows one to have both A and B objects on the slit.

### 5.2.2 Chopping parameters

The chopping technique, as described in § 3, is based on beam switching using the moving secondary mirror of the telescope. It allows to alternatively observe a field, then another field offset from the first by a chopping distance or throw, called `TEL.CHOP.THROW`, see Fig. 15. This parameter can be set by the user. To avoid chopping inside the object it is recommended to use a chopping and nodding throw which is ~ 1.5 times larger than the estimated `MIR` diameter of the object. In the case of point sources, the throw is usually set around ~10'' to ensure proper separation of the different beams. The maximum chopping throw at the VLT is 30'' and the minimum is 8''. For good image quality, and good background cancelation, chopping and nodding throws below 15'' are recommended (see § ??). *Note that for chopping throws larger than the field-of-view, the negative beams will not be seen on the detector, and the integration times have to be adjusted accordingly.*

The chopper position angle, *PA*, is the angle of chopping counted East of North (see Fig. 15). This parameter can be set by the observer. In order to keep the same distribution of beams on the detector for a different rotator angle (`TEL.ROT.OFFANGLE`) as in the default rotator position (see Fig. 17), then `TEL.CHOP.POSANG` must be equal to `TEL.ROT.OFFANGLE`. In particular, this is the case in spectroscopy if the observer wishes to have the 3 beams along the slit. As stated in § 3.5, the chopping frequency is not a parameter accessible to the observer, it is fixed internally to ensure the best data quality.

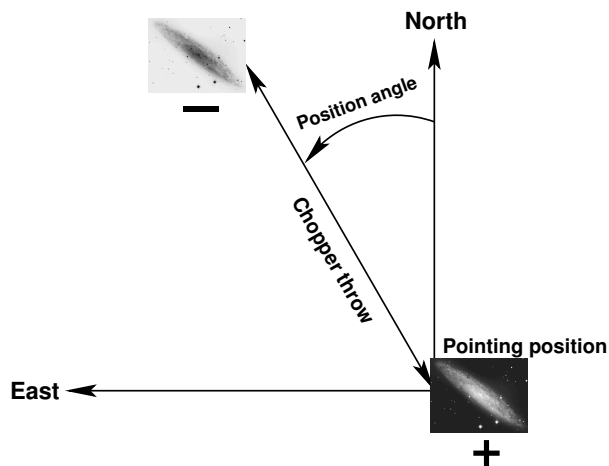


Figure 15: Definition of chopping parameters from the *telescope* point-of-view. If the position angle (*PA*) is measured counter-clockwise from North to East with *PA* between 0 and 360°, then `TEL.CHOP.POSANG` is  $360^\circ - \text{PA}$ . The positive beam (+) is obtained when the M2 is at Chopping Position A and corresponds to the pointing position of the telescope as given in the FITS header (idle position). The negative beam (-) is obtained by moving the M2 so that it points to a position angle on the sky given by *PA* and a throw of `TEL.CHOP.THROW` from the telescope pointing position (Chopping Position B). If `TEL.CHOP.POSANG` = `TEL.ROT.OFFANGLE` =  $360^\circ - \text{PA}$ , the resulting image on the detector will appear as in one of the nodding position images illustrated in Fig. 17.

### 5.2.3 Nodding parameters

The nodding technique allows to switch from one field to another by offsetting the telescope by several tens of arc-seconds. It allows to correct for optical path residuals that remain after chopping (§ 3).

The nodding period is a parameter that can only be modified by the instrument operator. For exposures shorter than 180s ( $SEQ.TIME < 180s$ ) – as possible in acquisition images –, the nodding time is set to half the requested exposure time. For exposures longer than 180s, the nodding time is set to 90s. *In particular, exposure time given in the template will be internally changed by the software to be the closest to a multiple of 90s.*

In all the 'AutoChopNod' templates, the nodding offset is equal to  $TEL.CHOP.THROW$  and cannot be modified.

In order to reach Nodding Position B, the telescope executes an offset of  $TEL.CHOP.THROW$ , along a position angle equal to

- $PA + 90^\circ = 360^\circ - TEL.CHOP.POSANG + 90^\circ$ , if  $SEQ.CHOPNOD.DIR = PERPENDICULAR$ ,
- $PA + 180^\circ = 180^\circ - TEL.CHOP.POSANG$ , if  $SEQ.CHOPNOD.DIR = PARALLEL$ .

The resulting distribution of images on a frame is illustrated in Fig.17. In imaging, more flexibility on the nodding offsets are possible with the `VISIR_img_obs_GenericChopNod` template.

## 5.3 Target acquisition

### 5.3.1 Introduction

Observing blocks (OB) must start with an acquisition template. Pointing to a target can only be performed through an acquisition template. The target coordinates, name and proper motion are all set in the acquisition templates.

The execution of the acquisition templates presets the telescope to the target coordinates given by  $TEL.TARG.ALPHA$  and  $TEL.TARG.DELTA$ . Offsets with respect to the target coordinates can be specified by  $TEL.TARG.OFFSETALPHA$  and  $TEL.TARG.OFFSETDELTA$  and allow, for example, to use a bright reference star for precise acquisition (see Fig. 16). To guarantee proper centering within the slit (when using a reference star) the angular separation between the reference star and the target should not be larger than 60". Acquisition with a reference star has not been tested with the narrow, 0.4" slit and should be avoided. Note that the coordinates of the target ( $TEL.TARG.ALPHA$ ,  $TEL.TARG.DELTA$ ) and the offsets to the reference star ( $TEL.TARG.OFFSETALPHA$ ,  $TEL.TARG.OFFSETDELTA$ ) must be indicated in the acquisition template. Thus, the following convention<sup>2</sup> :

$$TEL.TARG.ALPHA + TEL.TARG.OFFSETALPHA = RA(offsetstar),$$

$$TEL.TARG.DELTA + TEL.TARG.OFFSETDELTA = DEC(offsetstar).$$

will be used and the telescope is preseted to the reference star. Once the reference star is properly centered,  $TEL.TARG.OFFSETALPHA$  is subtracted back and the telescope is moved to the target.

---

<sup>2</sup>This convention is identical to the UVES one, but differs, from example, from the ISAAC or NACO one.

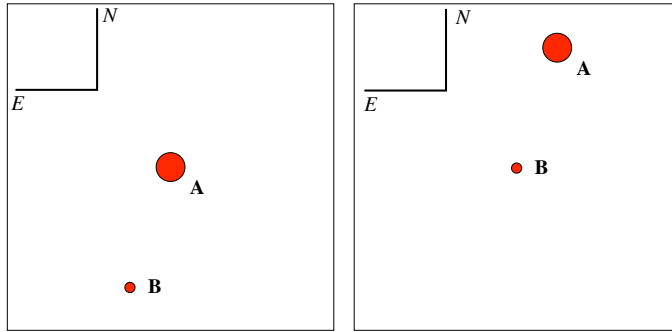


Figure 16: Setting the correct values of the `TEL.TARG.OFFSETALPHA` and `TEL.TARG.OFFSETDELTA` for a blind offset. Here the object A is a bright star used to center the target – the faint object B – at the center of the field. The telescope will first point at the object A. The instrument operator centers it properly. Once done, the telescope is offset so that object B is now properly centered and the observation templates can be executed. Following the convention described in the text, and since the target (object B) is at the east of the offset star, `TEL.TARG.OFFSETALPHA` is negative; on the other hand, the target is at the south of the offset star, so `TEL.TARG.OFFSETDELTA` is positive.

### 5.3.2 Description

There are two acquisition templates for imaging, `VISIR_img_acq_Preset` and `VISIR_img_acq_MoveToPixel`. One acquisition template is available for spectroscopy, `VISIR_spec_acq_MoveToSlit`. We emphasize that the `VISIR_spec_acq_ImgMoveToSlit` (which performed spectroscopic acquisition with the imager detector, and in principle allowed the possibility to acquire fainter objects in the old DRS detectors) is no longer offered. The observing parameters are described in § 9.

The effect of all acquisition templates is first to point the telescope so that the coordinates at the center of the detector match

- the target coordinates, if no blind offset is used,
- the offset star coordinates, otherwise,

within the accuracy of the VLT pointing (see below). For `VISIR_spec_acq_MoveToSlit`, the first acquisition images are obtained with the OPEN (15.3'') slit.

Then,

- The `VISIR_img_acq_MoveToPixel` and `VISIR_spec_acq_MoveToSlit` require interaction with the instrument operator or night support astronomer in order to center the target at the appropriate location on the detector. Without further indication given by the observer, the default locations are:
  - for `VISIR_img_acq_MoveToPixel` and `SEQ.CHOPNOD.DIR = PARALLEL`: 3'' North from the center of the detector to avoid the central-outward readout of the detector;
  - for `VISIR_img_acq_MoveToPixel` and `SEQ.CHOPNOD.DIR = PERPENDICULAR`: in the top left quadrant of the detector, at a distance equal to `TEL.CHOP.THROW/2` from the center of the detector in both X and Y;
  - for `VISIR_spec_acq_MoveToSlit`: at 3'' South from the center of the chosen slit;

In service mode, acquisition with the `VISIR_spec_acq_MoveToSlit` template is limited to objects brighter than 0.2 Jy.

All acquisition images are recorded and archived. Note that, *except if specifically requested in the README file*, photometric standard stars are not necessarily observed in the same filter as the acquisition filters.

As part of the execution of the `VISIR_spec_acq_MoveToSlit` template, an image used to measure the slit location is always taken and archived. In service mode, through slit images, obtained using the filter set by the `INS.FILT2.NAME` parameter, are also taken and archived so that the user can assess the correct centering of her/his object. The slit location image and the through–slit images are automatic procedures. Only the exposure time of the through–slit images can be modified by a service mode observer. Their execution time is included in the advertised execution time of the spectroscopic acquisition template.

- If the target coordinates are well known, VISIR imaging modes allow to perform blind preset observations with the `VISIR_img_acq_Preset` template. In this case, no acquisition images are taken.

By default, if `TEL.TARG.ALPHA` and `TEL.TARG.DELTA` contain the (accurate) coordinates of the target, the target will be located at the center of the detector, *including if the observing templates use* `SEQ.CHOPNOD.DIR = PERPENDICULAR`. In this case, in order to avoid to lose the chopnod images, it is advisable either to

- change the parameters `TEL.TARG.ALPHA` and `TEL.TARG.DELTA` so that they are offset by half the `TEL.CHOP.THROW` values, to south and west for `TEL.ROT.OFFANGLE = TEL.CHOP.POSANG = 0`;
- or use the parameters `TEL.TARG.OFFSETALPHA` and `TEL.TARG.OFFSETDELTA`: as above, the convention ‘final coordinates (RA, DEC) of the center of the field plus offsets equal initial coordinates’ is used, which translates into

$$RA + TEL.TARG.OFFSETALPHA = TEL.TARG.ALPHA,$$

$$DEC + TEL.TARG.OFFSETDELTA = TEL.TARG.DELTA.$$

Therefore, if `TEL.ROT.OFFANGLE = TEL.CHOP.POSANG = 0`, `TEL.TARG.OFFSETALPHA` and `TEL.TARG.OFFSETDELTA` should be positive in order to reproduce the scheme shown in Fig. 17. A typical value for these parameters is `TEL.CHOP.THROW/2`, where `TEL.CHOP.THROW` is the chop throw used in the subsequent templates.

If both the target and guide star coordinates are within the same astrometric systems, the pointing accuracy is limited by the relative accuracy between the coordinates of the two objects. In particular, the pointing accuracy maybe affected by significant (usually unknown) proper motion of the guide star. Note that the observatory does not guarantee the accuracy of the world coordinate systems (WCS) keywords in the FITS headers.

Acquisition with the `VISIR_img_acq_MoveToPixel` template can in principle make use of the K-Band filter, for which a preliminary conservative limiting magnitude is  $\sim 12$  in 60s on–source integration, for a  $S/N = 10$ . However, we strongly recommend to limit the acquisition filters to the N-band filters, as observations in the K-band filter employ the detector at starvation levels. Lastly, we emphasize that the K-band filter is not offered for science purposes.

For a successful completion of an OB, the observer has to ensure that correct target coordinates are provided for the equinox J2000.0 ideally at the epoch of the observations<sup>3</sup>. The following cases require special care:

- *imaging in the small field*: in some conditions, an error of less than 15'' on the coordinates can bring the target outside of the field;
- *spectroscopic acquisition*: in some conditions, an error of less than 7.5'' on the coordinates can bring the target outside of the wide, 15'', used slit.

Errors of such scale are common in the following situations:

- *high proper-motion stars*: in particular, if the epoch of the VISIR observations is significantly different from the epoch for which the coordinates were determined.
- *point-like sources within extended objects*: such as an AGN: a number of catalogues do not provide accurate coordinates of the nucleus. Coordinates given by 2MASS are more reliable.
- *coordinates obtained with low spatial resolution instrument*, such as MSX, etc...

For solar system objects, the J2000.0 equinox, topocentric, ICRF or FK5 coordinates at the epoch of the observations are required, as the Telescope Control System takes into account precession, nutation, annual aberration and refraction. On the contrary, the topocentric, *apparent* coordinates at the observatory, often used in other observatories, should *not* be used. Additional velocity parameters corresponding to  $\mu(\alpha) \cos \delta$  and  $\mu(\delta)$  must be given in ''/s.

## 5.4 Guide stars

Guide stars are mandatory for active optics and field stabilization. Any VLT program should make sure that a guide star (UCAC3) with a  $R = 11 - 13$  mag is available within a field of 7.5' around the object.

Sensitivity in the mid-IR for a ground based observatory is strongly limited by the sky brightness. In addition, the VISIR field is small compared to other VLT instruments. Therefore images of a field can often appear empty in short to medium length exposures. However, objects may become visible in longer ones. Combining different exposures taken on different nights may be tricky if a proper astrometric alignment is not carried out. Since the overall astrometric accuracy of an image is actually limited by the accuracy on the coordinates of the guide star, it is strongly recommended that all OBs of a same field use the *same* guide star, in particular for faint objects.

In addition, objects within (optically) dark molecular clouds may have few or no suitable guide stars, at least in the catalogues currently used by the Telescope Control System: the UCAC3. Alternatively, some bright nebulae may saturate the region of the digital sky surveys used by the telescope operator to select guide stars. Considerable amount of telescope time will be saved if such cases are identified *before* an OB is started.

Providing the coordinates of a guide star in the acquisition template of an OB is therefore strongly recommended in a number of situations:

- observations of faint objects, hardly or not visible even after a long exposure, in particular, if this exposure has to be combined with other ones;

---

<sup>3</sup>In particular, note that P2PP only accepts coordinates for J2000.0



- observations of objects within (optically) dark molecular clouds where few suitable guide stars are expected;
- observations of objects within bright nebulae larger than the field of view accessible by the guide-probe that appeared saturated in the digital sky surveys (example: Orion);
- observations for which astrometric accuracy is important.

In all these cases, the use of the guidecam tool (see <http://www.eso.org/instruments/visir/doc>) for VISIR is strongly recommended and the coordinates of a suitable guide star should be inserted in the acquisition templates.

If TEL.AG.GUIDESTAR is 'CATALOGUE', a guide star from the guide star catalog will be automatically selected by the TCS. If TEL.AG.GUIDESTAR is 'SETUPFILE', the observer has to provide the coordinates of the Guide Star. The coordinates of the guide star also fix the reference point for the World Coordinate System coordinates, that appear in the FITS header of the files.

In both cases, the telescope operator acknowledges the guide star. Depending on the weather conditions or if the star appears double in the guide probe, the telescope operator may have to select another guide star. Therefore, *if the observer has selected a guide star for astrometric purposes* – for example, to insure the repeatability of the pointings between different OBs –, *a clear note should be given in the README file, for service mode observations, or be specifically mentioned to the night time astronomer*, in visitor mode. As stated above, the observatory does not guarantee the accuracy of the world coordinate systems (WCS) keywords in the FITS headers.

## 5.5 Brightness limitations

There are currently no brightness limitations with VISIR. However, it is advised to observe only sources fainter than 500 Jy in N and 2500 Jy in Q to avoid detector artifacts (§ 4.4).

## 5.6 Overheads

The VLT overhead for one OB which includes active optics setting, selection of guide star, field stabilization is 6 min.

VISIR instrument configurations can be changed in a short time. For example a complete change of instrument settings takes less than 2 minutes. The total time for an image acquisition of a bright sources ( $> 1$  Jy) takes  $\sim 5$  min. for one fine acquisition iteration, or in blind preset 2 min. Spectroscopic acquisitions take longer and are strongly dependent on the source brightness : an overhead of 15 min. is accounted for sources  $> 1$  Jy, while 30 min. are required for sources between 0.2 and 1 Jy, respectively.

Instrument overheads due to chopping and nodding duty cycle losses are measured to be 50% of the observing time.

The total observing time requested by the observer must include telescope and instrument overheads.

## 5.7 Calibration observations

MIR observations depend strongly on the ambient conditions such as precipitable water vapor (PWV), temperature or airmass. In service mode science observations are interlaced by calibration observations on a timescale of 3h. Observations of photometric standards will be provided by the observatory within a time interval of three hours with respect to the science observations.

Calibrators, unless provided by the observer, are selected from the MIR spectro-photometric standard star catalog of the VLT (<http://www.eso.org/instruments/visir>). This catalog is a sub-set of the radiometric all-sky network of absolutely calibrated stellar spectra by Cohen et al.<sup>4</sup>. This list is supplemented by MIR standards used by TIMMI2 (see <http://www.ls.eso.org/lasilla/sciops/3p6/timmi/html/stand.html>).

At present the standard star catalog contains 425 sources. Zero point fluxes (Jy) have been calculated for the VISIR filter set by taking into account the measured transmission curves (Fig. 19), the detector efficiency and an atmosphere model (Fig. 2).

Continuous observations over 3 hours of the same standard star indicates that photometric stability better than 3% can be achieved with VISIR at the VLT. In order to test if a photometric precision of the same order can be obtained, a reduced set of standard stars has been built consisting of the Cohen et al. stars which obey the following criteria:

- visibility from Paranal;
- no variability detected by Hipparcos non-variables (Var = 0 in the Hipparcos catalogue);
- absolute flux calibration errors (as reported by Cohen et al.) < 20%;
- all spectral types reported in SIMBAD no more than 1 sub-class different from that used by Cohen et al.;
- not visual binaries (as reported by SIMBAD).

This catalogue of 81 stars is also made available at <http://www.eso.org/instruments/visir>.

From this catalogue, a further selection to provide a reduced list of 12 stars has been carried out (see also <http://www.eso.org/instruments/visir>). These stars are distributed as uniformly as possible in Right Ascension, with spectral types as similar as possible. In addition, their flux in the N band, of the order of 10Jy, is bright enough to be observable in the Q band without reaching non-linearity levels in the N band even in non-ideal background conditions. At least one star in this reduced catalogue will be observed every night VISIR is in use. Note that this list could be modified without previous notice.

A PSF can be derived from these photometric standard star observations. However, it is not guaranteed that its S/N is sufficient for deconvolution purposes. If the observer requires a specific PSF measurement, (s)he has to provide the corresponding PSF OB.

Observations of photometric standards provided by the observatory are taken using the VISIR\_img\_cal\_AutoChopNod template (§ 7) with the following settings:

---

<sup>4</sup>Cohen et al., 1999, AJ 117, 1864

|                 |                                      |
|-----------------|--------------------------------------|
| SEQ.TIME        | 180 sec for N and 360 sec for Q band |
| TEL.CHOP.POSANG | 0°                                   |
| TEL.CHOP.THROW  | 10''                                 |
| SEQ.CHOPNOD.DIR | PERPENDICULAR                        |

Filter INS.FILT1.NAME and pixel scale INS.PFOV will be set according to the science observations.

In spectroscopy, the observatory will provide spectro-photometric observations of a telluric (K or M type) standard star in the Low Resolution mode, based on the same catalog as for imaging with an airmass difference no larger than 0.2 AM respect to the science target. Such a calibration measurement will be performed at least once per night, per instrument configuration. More precisely the following settings of the VISIR\_spec\_cal\_LRAutoChopNod template (§ 7) will be used:

|                 |          |
|-----------------|----------|
| SEQ.TIME        | 180 sec  |
| TEL.CHOP.POSANG | 0°       |
| TEL.CHOP.THROW  | 8''      |
| SEQ.CHOPNOD.DIR | PARALLEL |

The INS.SLIT1.WIDTH will be adjusted according to the science observation.

Important note:

The observatory does **not** provide standard calibrations for VISIR medium and high resolution spectroscopy. Thus for medium and high resolution mode the observer has to supply his own calibration by supplying a calibration OB to each science OB. The observing time needed to execute this calibration is charged to the observer. Ideally, early type stars should be chosen. In particular, for high resolution spectroscopy, asteroids provide mostly featureless spectra on the VISIR spectral range.

For service-mode observations, all Calibrator Observations should be Concatenated to their science OB. In addition, the "DIT determination Algorithm" should be set to "AUTO" or "BRIGHT-SOURCE" for the first occurrence of each filter or wavelength setting, and it should be set to "PREVIOUS" in all subsequent observing template.

For both imaging and spectroscopy, day calibrations of VISIR are performed with an extended source that mimics a black-body with adjustable flux (by regulating its temperature). For most instrument modes, a corresponding flat-field is recorded, which consists of a series of images with different background levels. Exceptions are: SiC in the Intermediate Field and all imaging obtained with the spectroscopy detector (for spectroscopy acquisition). Bad pixels, gain maps and fringing patterns can, in principle, be derived from these flat-fields. However, at the moment, the scientific value of the application of these corrections is not established. These day calibrations are supplied to the user on an experimental basis and may be discontinued with no previous notice.

## 5.8 OBs Classification

The sky transparency constraints used at Paranal are: photometric (PHO), clear (CLR), thin (THN), and thick (THK). They mostly refer to the optical band and their translation to the IR domain, and specially to the MIR, is not obvious. The following scheme is applied for VISIR. OBs requiring PHO conditions will be executed and classified as A (Fully within constraints) if the sensitivity in the corresponding band is equal or better then the nominal median value and if the conversion factor is constant within 10%. Refer to the web page <http://www.eso.org/instruments/visir/inst/> to know the values of nominal sensitivities in each mode. OBs requiring CLR, THN and THK

conditions will be executed and classified as A when the sensitivity is respectively within 20%, 30% and 50% the nominal values.

Classification for VISIR observations conducted in service-mode is also based on the PWV constraint. OBs executed with the requested PWV constraint will be classified A (Fully within constraints), those executed within 10% of the requested PWV value will be classified B (Almost within constraints) and OBs executed under PWV conditions greater than 10% of the requested PWV value will be classified C (out of constraints). Observations qualified as "C" will be repeated. The time required to do so will not be charged to the observer's program.

## 5.9 Known problems

The cosmetic quality of the AQUARIUS detector is very good. However, this and eventual other problems (e.g. decreased image quality, bad residuals, stripes etc) still need to be investigated. We emphasize that due to the central-outward readout of the Imager and Spectrometer detectors, the science targets need to avoid the central 20 pixels horizontal stripe around Y=512.

## 6 VISIR data

### 6.1 Data format

One FITS file is saved for each telescope nodding position. This file is a data multi-extension fits file and contains for each chopping cycle:

1. general header
2. each half cycle frame of the on-source position (A) of the chopper,
3. the average of the current and all previous(A-B) chopped frames,

In addition, the last extension of the file contains the average of all chopped frames.

In Burst mode a number of FITS files is saved. Each file is a data cube containing up to 1500 elementary frames. The total number of files is such that it sums up the total integration time requested. For the default value of the rotator angle (0°), images are oriented North up and East left. Spectroscopic data are aligned horizontally in the spatial and vertically in the dispersion direction (cf. Fig.??). For the LR and MR modes, the short wavelength appear at the top of the frames. For the HR and HRX modes, the short wavelength is at the top of the frame if the side B of the dual-grating is used, and at the bottom of the frame of the side A is used.

### 6.2 Pipeline

A pipeline for the reduction of VISIR data has been developed by ESO. The main observation templates are supported by the pipeline reductions. Raw images of imaging and spectroscopic observations are recombined. Spectra are extracted and calibrated in wavelength (§ 6.3) for all spectroscopic modes in low-, medium-, and high-resolution. Sensitivity estimates based on standard star observations are provided both in imaging and spectroscopy (§ 5.7). The public release of the VISIR pipeline is accessible at: <http://www.eso.org/sci/software/pipelines/>.

The pipeline currently supports the following templates :

- VISIR\_img\_obs\_AutoChopNod
- VISIR\_spec\_obs\_LRAutoChopNod
- VISIR\_spec\_obs\_MRAutoChopNod
- VISIR\_spec\_obs\_HRAutoChopNod
- VISIR\_spec\_obs\_HRXAutoChopNod
- VISIR\_img\_obs\_BurstAutoChopNod

In mosaic (or raster) mode (VISIR\_img\_obs\_GenericChopNod) only raw frames are delivered, e.g. mapping reconstruction algorithms are not supported.

## 6.3 VISIR spectrometer data

### Optical distortion correction

Spectra are deformed by optical distortion and slit curvatures. The VISIR spectrograph uses curved slits to cancel the distortion of the pre-slit optics. Thus the slit projected on the sky is straight. There is an additional linear distortion in both dispersion and cross-dispersion direction of the detector. The distortions have not been estimated yet for the new AQUARIUS detector, and will be reported after the full commissioning of the new detectors.

### Wavelength calibration

A first order wavelength calibration is given by the optical model of the instrument. Its precision is about  $\pm 10$  pixels for the low and medium resolution mode and  $\pm 15$  pixels for the high resolution mode. The wavelength calibration can be refined by using Fabry-Perot Etalons plates or atmospheric lines. In the VISIR extensions file, chopper half-cycle frames, which are dominated by sky emission lines, are stored (§ 6.1). They can be used to fine-tune the wavelength calibration to sub-pixel precision by comparison with a model of the atmospheric lines. This method is used by the pipeline. More specifically, the zero-point of the wavelength calibration is obtained by cross-correlating the observed sky spectrum with a HITRAN model of the sky emission lines.

The chopped frames cannot be used for calibration with atmospheric lines because the chopping process results in a near perfect cancelation of sky lines.

### Atmosphere absorption correction

The atmosphere does not uniformly absorb the MIR radiation (§ 3.1). At some wavelengths it is completely transparent, at others partly or completely opaque. Differential absorption is often corrected by dividing the extracted spectrum by a reference spectrum. This procedure may cause numerical instabilities at wavelengths close to strong sky lines that might amplify the noise.

### Photometry

Spectro-photometric calibration of low and medium resolution spectra can be achieved with the MIR standard star list provided by the Observatory (see § 5.7). For high-resolution spectroscopy only calibrators known with high precision, such as, A stars or asteroids, should be considered. However, even early A stars are known to have some hydrogen absorption lines in the N and Q band.

## 7 VISIR templates description

### 7.1 Acquisition

Each OB needs to start with an acquisition template, they are described in § 5.3.

### 7.2 Observing with the imager

VISIR\_img\_obs\_AutoChopNod

This template permits observing a source in imaging configuration with various sub-settings. The observer must specify filter, pixel scale, chopper throw, which is in the range of 8'' to 30''. The keyword SEQ.CHOPNOD.DIR is set to PARALLEL or PERPENDICULAR, which results in images as shown in Fig. 17. PARALLEL considers an equal nodding and chopping amplitude which are both in parallel direction. It is recommended for faint, extended sources, for which the spatial resolution is not so crucial. PERPENDICULAR considers an equal nodding and chopping amplitude; however in perpendicular direction. Note that while the telescope offset is in positive (East) direction, the resulting image on the detector will move to the West. This technique is recommended for point or relatively small extended (< 5'') sources (Fig. 5).

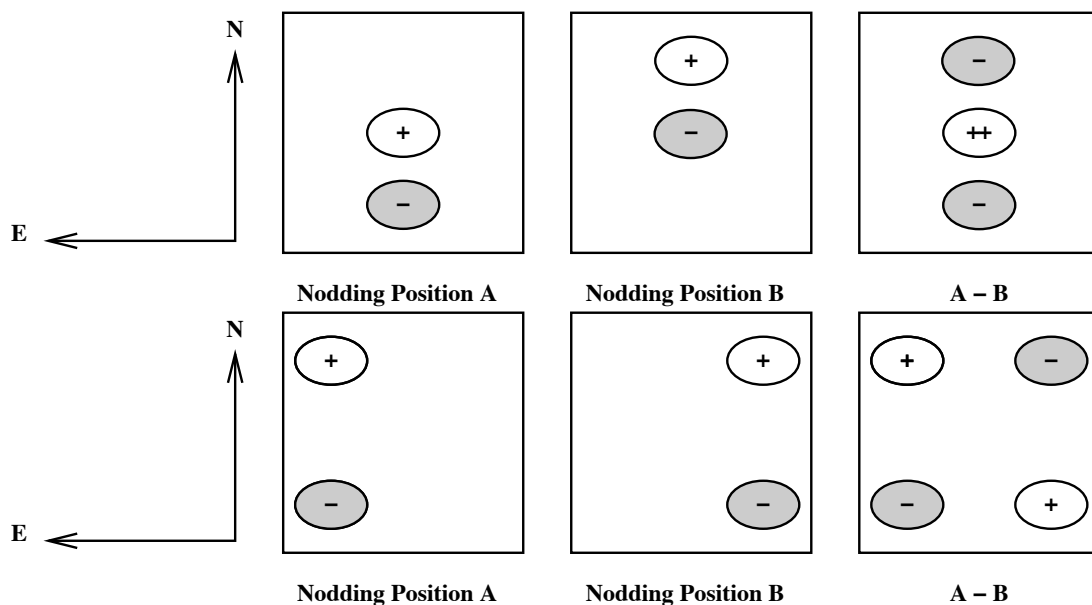


Figure 17: Schematic drawing of the content of a frame obtained with TEL.ROT.OFFANGLE = TEL.CHOP.POSANG = 0 and SEQ.CHOPNOD.DIR = PARALLEL (top) and SEQ.CHOPNOD.DIR=PERPENDICULAR (bottom). In the individual nodding positions, the positive beams correspond to the chopper position A and the negative beams to the chopper position B. Note that the default pointing position of the telescope corresponds to the center of the detector. Within the accuracy of the telescope pointing, this location matches the nodding position A, chopper position A if SEQ.CHOPNOD.DIR = PARALLEL.

The keywords SEQ.JITTER.WIDTH allows chopping and nodding with random offsets so that a jitter pattern is performed. This technique allows to reconstruct bad pixels. For SEQ.JITTER.WIDTH = 0 no jitter is performed and the resulting image depends on the setting of SEQ.CHOPNOD.DIR. The chopping period is set by the system and the nodding period is fixed to 90 s. The number of nodding

cycles  $N_{cycl\_nod}$  is computed according to the total observation time (§ 4.5).

### VISIR\_img\_obs\_GenericChopNod

This imaging template enhances the flexibility of nodding offsets, and allows the user to specify them in a list of relative offset positions. In the most simple application, only one offset position is specified. This allows to record nodding pairs, i.e. cycle of on–off observations, using a flexible offset position. Additional jitter offsets can be specified. More than one entry in the offset list results in a freely programmable pattern of nodding pairs. Note that the integration time, SEQ.TIME, specified refers to only one nodding pair. The total observing time is given by the product of SEQ.NOFF  $\times$  SEQ.TIME. The offset positions are calculated as the cumulative sum of offsets, i.e. are defined relative to the previous offset positions. Note that the telescope always returns to the first (reference) position, when specifying a list of offsets. This mode can be exploited to perform mosaic or raster imaging. The first reference position can then be considered as a sky observation while the offsets refer to object positions. It is recommended to offset to positions that result in observations of overlapping fields, which enhances the redundancy after image reconstruction.

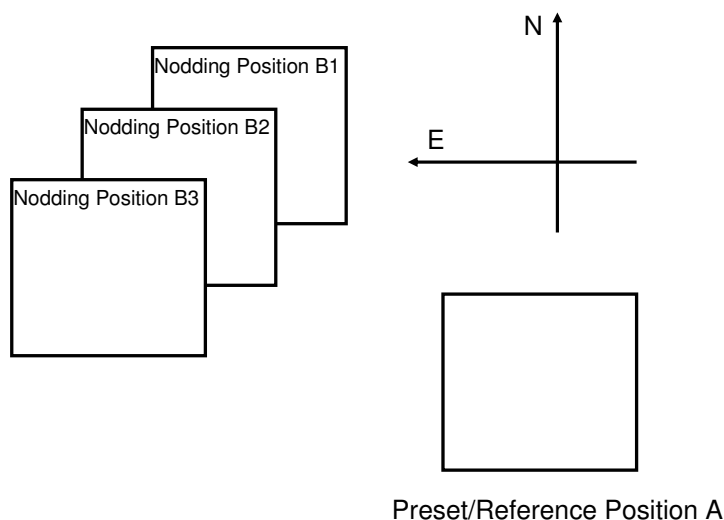


Figure 18: Illustration of generating raster maps with VISIR\_img\_obs\_GenericChopNod.

An illustration of generating an raster map can be found in Fig. 18. The following parameters correspond to this setting:

```
SEQ.NOFF          3
SEQ.OFFSET1.LIST  30 10 10
SEQ.OFFSET2.LIST  30 -10 -10
SEQ.OFFSET.COORDS SKY
```

Note that depending on choice of the integration time `SEQ.TIME`, several nodding cycles might result, e.g. pattern like `AB1B1AAB1B1A..AB2B2AAB2B2A..AB3B3AAB3B3A`.

Currently, images obtained with the `VISIR_img_obs_GenericChopNod` are not reduced by the ESO VISIR pipeline.

*Pre-imaging observations:* Since Period 76, the observatory supports a fast data release for VISIR pre-imaging observations. Pre-imaging images must be obtained either with the `VISIR_img_obs_AutoChopNod` or `VISIR_img_obs_GenericChopNod` templates. The `SEQ.CATG` keyword must be set to `PRE-IMAGE`. In addition, the name of the OB must start with the prefix `PRE`.

#### `VISIR_img_obs_BurstAutoChopNod`

The observations in burst mode are analogous to the observations with the template

`VISIR_img_obs_AutoChopNod` but single elementary frames are saved. These can be single DIT frames or the average of a number NDIT of DIT frames. The minimum total integration time is 2 minutes and the total integration time must be a multiple of this value. NDIT can assume values from 1 to 10.

### 7.3 Observing with the spectrometer

Conceptually the same observing techniques applies for spectroscopy as well as for imaging. The default slit orientation is in North-South direction. The length of the slit is selected by the keyword `INS.SLIT1.TYPE`: only for cross-dispersed, high-resolution, observations `SHORT` must be used, otherwise `LONG` is the default setting.

A preferred observing strategy is called "nodding on the slit", where the chopping and nodding amplitudes are small (`SEQ.CHOPNOD.DIR = PARALLEL`). Note that "nodding on the slit" requires to set the telescope rotator offset angle *and* the M2 chopping position angle to the same value (which is, in general, different from 0). This is useful to acquire two targets simultaneously in the slit.

The keyword `SEQ.JITTER.WIDTH` allows to apply random offsets *along the slit*.

More complex source geometries might require larger amplitudes, and/or `SEQ.CHOPNOD.DIR = PERPENDICULAR` in order to avoid self-cancellation.

#### **Low and medium resolution**

Templates for low and medium resolution spectroscopy are:

`VISIR_spec_obs_LRAutoChopNod` and `VISIR_spec_obs_MRAutoChopNod`, respectively. Observing parameters are: total integration time (`SEQ.TIME`), central wavelength (`INS.GRAT1.WLEN`), the slit width `INS.SLIT1.WIDTH` and `SEQ.CHOPNOD.DIR` (§ 7.2).

#### **High resolution: long-slit mode**

The template for high resolution spectroscopy is `VISIR_spc_obs_HRAutoChopNod`. Three order sorting filter at 8.02, 12.81 and 17.03 $\mu\text{m}$ , `INS.FILT2.NAME = ([H2_S4],[Ne II],[H2_S1])` are available. The effective length of the spectrograph slit is limited to 32".5. See Table 6 for the corresponding list of offered central wavelengths. Other observing parameters are: total integration time (`SEQ.TIME`), central wavelength (`INS.GRAT1.WLEN`), the slit width (`INS.SLIT1.WIDTH`) and `SEQ.CHOPNOD.DIR` (§ 7.2).



**High resolution: cross-dispersed mode**

VISIR\_spc\_obs\_HRXAutoChopNod is functionally similar to VISIR\_spc\_obs\_HRAutoChopNod, but uses a grism for cross-dispersion and order-separation. See Table 6 for a list of offered wavelengths. Note that the effective length of the spectrograph slit is limited to  $\sim 4''$ . Total integration time (SEQ.TIME), the slit width (INS.SLIT1.WIDTH) and SEQ.CHOPNOD.DIR are specified as usual (§ 7.2).

**7.4 Calibration**

Specific templates exist for the observations of photometric and spectro-photometric standard stars. They offer the same functionality as the corresponding science templates, but allow to monitor the sensitivity and image quality by observing calibration standard stars.

Their use is recommended to be properly recognized by the VISIR pipeline.

## 8 Checklist

This section provides a number of advice regarding the preparation of the proposal.

### 8.1 Phase 1

It is very important that the time justification (Box 9) of the proposal contains enough information so that its feasibility can be correctly assessed. The following points must be respected:

1. the expected S/N for each object and modes must be given;
2. in particular for extended sources: does the reported S/N refer to an area of  $1 \text{ arcsec}^2$  (as given by the imaging ETC), to an extent of 1 arcsec in the spatial direction (as given by the spectroscopy ETC) or to the whole spatial extent of the object?
3. in spectroscopy, does the S/N refer to one pixel in the dispersion direction (as given by the ETC) or to one resolution element?
4. in case of large throw, does the S/N take into account the fact that some beams would fall outside the detector?
5. does the overhead calculation include the time required for each preset, given that OBs should in general not be longer than 1 hour?
6. is there a guide star brighter than  $V = 13.5$  mag within a radius of 7.5 arcmin around the object?
7. The PWV constraint under which the observations need to be executed needs to be specified as a comment in the Target List of the proposal.

### 8.2 Phase 2

1. *Acquisition:* Are the coordinates accurate in the equinox J2000.0 reference frame? For high-proper motion objects, are they valid for the epoch of the observations? For solar system objects, are they in the topocentric, ICRF or FK5, J2000.0 reference frame at the epoch of the observations?
2. *Acquisition:* If the `VISIR_img_acq_Preset` is used and the following templates have `SEQ.CHOPNOD.DIR = PERPENDICULAR`, the target will appear at the center of the detector by default, with the risk of losing 3 beams that would appear outside of the field. Either slightly change the coordinates of `TEL.TARG.ALPHA` and `TEL.TARG.DELTA`, or use `TEL.TARG.OFFSETALPHA` and `TEL.TARG.OFFSETDELTA`. See § 5.3.
3. *Acquisition:* It is strongly recommended that a same guide star be selected and inserted in the acquisition template for all OBs of a same field, in particular if
  - relatively good astrometric accuracy is required;
  - the object is faint or diffuse and unlikely to be visible on short exposures;
  - the object appears in the field of a bright nebula that saturates the digitized sky survey (DSS) used by the telescope and instrument operator;

The guidecam tool (see <http://www.eso.org/instruments/visir/doc>) can help in selecting appropriate guide stars.

4. *Calibrations:* For calibration OBs, use the appropriate `VISIR_img_cal_AutoChopNod` or `VISIR_spc_cal_LR/MR/HR/HRXAutoChopNod` templates.
5. *Position angle:* If the observations must be carried out at a position angle different from 0, check § 5.2.1 and § 5.2.2. In particular, it is useful to clearly indicate in the README file if `TEL.CHOP.POSANG` is not equal to `TEL.ROT.OFFANGLE` to warn the instrument operator about the non-standard configuration. In particular, in spectroscopy, `TEL.CHOP.POSANG` must be equal to `TEL.ROT.OFFANGLE` in order to have the 3 beams along the slit.

## 9 Appendix: VISIR template parameters

| VISIR_img_acq_MoveToPixel.tsf |   |   |
|-------------------------------|---|---|
| <i>To be specified:</i>       |   |   |
| Parameter                     | Range ( <i>Default</i> )  | Label   |
| <b>INS.FILT1.NAME</b>         | K-BAND SIC PAH1 ARIII<br>SIV_1 SIV SIV_2 PAH2<br>PAH2_2 NEII_1 NEII<br>NEII_2 Q1 Q2 Q3 ( <i>NODE-<br/>FAULT</i> ) | Imager Filter                                 |
| <b>INS.PFOV</b>               | 0.045 0.076 ( <i>0.076</i> )  | Imager pixel scale                            |
| <b>SEQ.CHOPNOD.DIR</b>        | PARALLEL PERPENDICU-<br>LAR ( <i>PARALLEL</i> )   | Relative Chop/Nod Direction                   |
| <b>SEQ.TIME</b>               | 30..3600 ( <i>NODEFAULT</i> )   | Total integration time (sec)                  |
| <b>SEQ.DIT.ALGO</b>           | AUTO, GOOD-WEATHER,<br>BRIGHT-SOURCE ( <i>NODE-<br/>FAULT</i> )   | DIT determination algorithm                   |
| <b>TEL.CHOP.POSANG</b>        | 0..359 ( <i>0</i> )   | Chopping Position Angle<br>(deg)              |
| <b>TEL.CHOP.THROW</b>         | 8..30 ( <i>8</i> )  | Chopping Amplitude (arcsec)                   |
| <b>TEL.GS1.ALPHA</b>          | ra ()   | Guide star RA                                 |
| <b>TEL.GS1.DELTA</b>          | dec ()  | Guide star DEC                                |
| <b>TEL.ROT.OFFANGLE</b>       | 0..359 ( <i>0.0</i> )   | Rotator on Sky (=PA on Sky)                   |
| <b>TEL.TARG.ADDVELALPHA</b>   | ( <i>0.0</i> )  | RA additional tracking veloc-<br>ity ("/sec)  |
| <b>TEL.TARG.ADDVELDELTA</b>   | ( <i>0.0</i> )  | DEC additional tracking ve-<br>locity ("/sec) |
| <b>TEL.TARG.ALPHA</b>         | ra ()   |   |
| <b>TEL.TARG.DELTA</b>         | dec ()  |   |
| <b>TEL.TARG.EQUINOX</b>       | ( <i>2000.0</i> )   |   |
| <b>TEL.TARG.OFFSETALPHA</b>   | ( <i>0.0</i> )  | RA blind offset                               |
| <b>TEL.TARG.OFFSETDELTA</b>   | ( <i>0.0</i> )  | DEC blind offset                              |

**VISIR\_img\_acq\_Preset.tsf**

*To be specified:*

| Parameter                   | Range (Default)                         | Label                                    |
|-----------------------------|---|--|
| <b>TEL.AG.GUIDESTAR</b>     | CATALOGUE SETUPFILE<br>NONE (CATALOGUE) | Get Guide Star from                      |
| <b>TEL.GS1.ALPHA</b>        | ra ()                                   | Guide star RA                            |
| <b>TEL.GS1.DELTA</b>        | dec ()                                  | Guide star DEC                           |
| <b>TEL.ROT.OFFANGLE</b>     | 0..359 (0.0)                            | Rotator on Sky (=PA on Sky)              |
| <b>TEL.TARG.ADDVELALPHA</b> | (0.0)                                   | RA additional tracking velocity ("/sec)  |
| <b>TEL.TARG.ADDVELDELTA</b> | (0.0)                                   | DEC additional tracking velocity ("/sec) |
| <b>TEL.TARG.ALPHA</b>       | ra ()                                   |  |
| <b>TEL.TARG.DELTA</b>       | dec ()                                  |  |
| <b>TEL.TARG.EQUINOX</b>     | (2000.0)                                |  |
| <b>TEL.TARG.OFFSETALPHA</b> | 0.0                                     | RA blind offset                          |
| <b>TEL.TARG.OFFSETDELTA</b> | 0.0                                     | DEC blind offset                         |

**VISIR\_spec\_acq\_MoveToSlit.tsf**

*To be specified:*

| Parameter                   | Range (Default)                               | Label                                    |
|-----------------------------|---|--|
| <b>INS.FILT2.NAME</b>       | N_SW N_LW ARIII NEII_1<br>NEII_2 (NODEFAULT)  | Acquisition Filter                       |
| <b>INS.SLIT1.TYPE</b>       | LONG SHORT (LONG)                             | Spectrometer Slit Type (long or short)   |
| <b>INS.SLIT1.WIDTH</b>      | 0.40 0.75 1.00 (NODEFAULT)                    | Spectrometer Slit Width (arcsec)         |
| <b>SEQ.CHOPNOD.DIR</b>      | PARALLEL PERPENDICULAR (PARALLEL)             | Relative Chop/Nod Direction              |
| <b>SEQ.TIME</b>             | 30..3600 (NODEFAULT)                          | Total integration time (sec)             |
| <b>SEQ.DIT.ALGO</b>         | AUTO, GOOD-WEATHER, BRIGHT-SOURCE (NODEFAULT) | DIT determination algorithm              |
| <b>TEL.CHOP.POSANG</b>      | 0..359 (0)                                    | Chopping Position Angle (deg)            |
| <b>TEL.CHOP.THROW</b>       | 8..30 (8)                                     | Chopping Amplitude (arcsec)              |
| <b>TEL.GS1.ALPHA</b>        | ra ()   | Guide star RA                            |
| <b>TEL.GS1.DELTA</b>        | dec ()  | Guide star DEC                           |
| <b>TEL.ROT.OFFANGLE</b>     | 0..359 (0.0)                                  | Rotator on Sky (=PA on Sky)              |
| <b>TEL.TARG.ADDVELALPHA</b> | (0.0)   | RA additional tracking velocity ("/sec)  |
| <b>TEL.TARG.ADDVELDELTA</b> | (0.0)   | DEC additional tracking velocity ("/sec) |
| <b>TEL.TARG.ALPHA</b>       | ra ()   |  |
| <b>TEL.TARG.DELTA</b>       | dec ()  |  |
| <b>TEL.TARG.EQUINOX</b>     | (2000.0)                                      |  |
| <b>TEL.TARG.OFFSETALPHA</b> | (0.0)   | RA blind offset                          |
| <b>TEL.TARG.OFFSETDELTA</b> | (0.0)   | DEC blind offset                         |

## 9.1 Observation

| <b>VISIR_img_obs_AutoChopNod.tsf</b>    |  |                              |
|---|--|------------------------------|
| <i>To be specified:</i>                 |  |                              |
| Parameter                               | Range ( <i>Default</i> )   | Label                        |
| <b>INS.FILT1.NAME</b>                   | SIC PAH1 ARIII SIV_1<br>SIV SIV_2 PAH2 PAH2_2<br>NEII_1 NEII NEII_2 Q1 Q2<br>Q3 ( <i>NODEFAULT</i> ) | Imager Filter                |
| <b>INS.PFOV</b>                         | 0.045 0.076 ( <i>0.076</i> )   | Imager pixel scale           |
| <b>SEQ.CATG</b>                         | PRE-IMAGE SCIENCE<br>( <i>SCIENCE</i> )  | Observation Category         |
| <b>SEQ.CHOPNOD.DIR</b>                  | PARALLEL PERPENDICU-<br>LAR ( <i>PARALLEL</i> )  | Relative Chop/Nod Direction  |
| <b>SEQ.JITTER.WIDTH</b>                 | 0..10 ( <i>0</i> )   | Random Jitter Width (arcsec) |
| <b>SEQ.TIME</b>                         | 180..3600 ( <i>NODEFAULT</i> )   | Total integration time (sec) |
| <b>SEQ.DIT.ALGO</b>                     | AUTO, GOOD-WEATHER,<br>BRIGHT-SOURCE ( <i>NODE-<br/>FAULT</i> )                                      | DIT determination algorithm  |
| <b>TEL.CHOP.THROW</b>                   | 8..30 ( <i>8</i> )   | Chopping Amplitude (arcsec)  |
| <b>VISIR_img_obs_GenericChopNod.tsf</b> |  |                              |
| <i>To be specified:</i>                 |  |                              |
| Parameter                               | Range ( <i>Default</i> )   | Label                        |
| <b>INS.FILT1.NAME</b>                   | SIC PAH1 ARIII SIV_1<br>SIV SIV_2 PAH2 PAH2_2<br>NEII_1 NEII NEII_2 Q1 Q2<br>Q3 ( <i>NODEFAULT</i> ) | Imager Filter                |
| <b>INS.PFOV</b>                         | 0.045 0.076 ( <i>0.076</i> )   | Imager pixel scale           |
| <b>SEQ.CATG</b>                         | PRE-IMAGE SCIENCE<br>( <i>SCIENCE</i> )  | Observation Category         |
| <b>SEQ.NOFF</b>                         | 1..100 ( <i>NODEFAULT</i> )  | Number of offset positions   |
| <b>SEQ.OFFSET.COORDS</b>                | SKY DETECTOR ( <i>NODE-<br/>FAULT</i> )  | Offset coordinates           |
| <b>SEQ.OFFSET1.LIST</b>                 | ( <i>NODEFAULT</i> )   | List of offsets in RA or X   |
| <b>SEQ.OFFSET2.LIST</b>                 | ( <i>NODEFAULT</i> )   | List of offsets in DEC or Y  |
| <b>SEQ.TIME</b>                         | 180..3600 ( <i>NODEFAULT</i> )   | Total integration time (sec) |
| <b>SEQ.DIT.ALGO</b>                     | AUTO, GOOD-WEATHER,<br>BRIGHT-SOURCE ( <i>NODE-<br/>FAULT</i> )                                      | DIT determination algorithm  |
| <b>TEL.CHOP.THROW</b>                   | 8..30 ( <i>10</i> )  | Chopping Amplitude (arcsec)  |

**VISIR\_spec\_obs\_LRAutoChopNod.tsf**

*To be specified:*

| Parameter               | Range (Default)                               | Label                             |
|-------------------------|---|-----------------------------------|
| <b>INS.GRAT1.WLEN</b>   | 10.5 (NODEFAULT)                              | Spectrometer Wavelength (microns) |
| <b>SEQ.CHOPNOD.DIR</b>  | PARALLEL PERPENDICULAR (PARALLEL)             | Relative Chop/Nod Direction       |
| <b>SEQ.JITTER.WIDTH</b> | 0..10 (0)                                     | Random Jitter Width (arcsec)      |
| <b>SEQ.TIME</b>         | 180..3600 (NODEFAULT)                         | Total integration time (sec)      |
| <b>SEQ.DIT.ALGO</b>     | AUTO, GOOD-WEATHER, BRIGHT-SOURCE (NODEFAULT) | DIT determination algorithm       |
| <b>TEL.CHOP.THROW</b>   | 8..30 (8)                                     | Chopping Amplitude (arcsec)       |

**VISIR\_spec\_obs\_MRAutoChopNod.tsf**

*To be specified:*

| Parameter               | Range (Default)                               | Label                             |
|-------------------------|---|-----------------------------------|
| <b>INS.GRAT1.WLEN</b>   | 7.5..28.08 (NODEFAULT)                        | Spectrometer Wavelength (microns) |
| <b>SEQ.CHOPNOD.DIR</b>  | PARALLEL PERPENDICULAR (PARALLEL)             | Relative Chop/Nod Direction       |
| <b>SEQ.JITTER.WIDTH</b> | 0..10 (0)                                     | Random Jitter Width (arcsec)      |
| <b>SEQ.TIME</b>         | 180..3600 (NODEFAULT)                         | Total integration time (sec)      |
| <b>SEQ.DIT.ALGO</b>     | AUTO, GOOD-WEATHER, BRIGHT-SOURCE (NODEFAULT) | DIT determination algorithm       |
| <b>TEL.CHOP.THROW</b>   | 8..30 (8)                                     | Chopping Amplitude (arcsec)       |

**VISIR\_spec\_obs\_HRAutoChopNod.tsf**

*To be specified:*

| Parameter               | Range (Default)                               | Label                             |
|-------------------------|---|-----------------------------------|
| <b>INS.FILT2.NAME</b>   | NEII_2 H2S_1 H2S_4 (NEII_2)                   | Spectrometer Filter               |
| <b>INS.GRAT1.WLEN</b>   | 7.80..19.18 (12.810)                          | Spectrometer Wavelength (microns) |
| <b>SEQ.CHOPNOD.DIR</b>  | PARALLEL PERPENDICULAR (PARALLEL)             | Relative Chop/Nod Direction       |
| <b>SEQ.JITTER.WIDTH</b> | 0..10 (0)                                     | Random Jitter Width (arcsec)      |
| <b>SEQ.TIME</b>         | 180..3600 (NODEFAULT)                         | Total integration time (sec)      |
| <b>SEQ.DIT.ALGO</b>     | AUTO, GOOD-WEATHER, BRIGHT-SOURCE (NODEFAULT) | DIT determination algorithm       |
| <b>TEL.CHOP.THROW</b>   | 8..30 (8)                                     | Chopping Amplitude (arcsec)       |

**VISIR\_spec\_obs\_HRXAutoChopNod.tsf**

| <i>To be specified:</i> |  |                                   |
|-------------------------|--|-----------------------------------|
| Parameter               | Range ( <i>Default</i> )                               | Label                             |
| <b>INS.GRAT1.WLEN</b>   | 7.60..28.08 ( <i>NODEFAULT</i> )                       | Spectrometer Wavelength (microns) |
| <b>SEQ.CHOPNOD.DIR</b>  | PARALLEL PERPENDICULAR ( <i>PARALLEL</i> )             | Relative Chop/Nod Direction       |
| <b>SEQ.JITTER.WIDTH</b> | 0..10 ( <i>0</i> )                                     | Random Jitter Width (arcsec)      |
| <b>SEQ.TIME</b>         | 180..3600 ( <i>NODEFAULT</i> )                         | Total integration time (sec)      |
| <b>SEQ.DIT.ALGO</b>     | AUTO, GOOD-WEATHER, BRIGHT-SOURCE ( <i>NODEFAULT</i> ) | DIT determination algorithm       |
| <b>TEL.CHOP.THROW</b>   | 8..30 ( <i>8</i> )                                     | Chopping Amplitude (arcsec)       |

## 9.2 Calibration

**VISIR\_img\_cal\_AutoChopNod.tsf**

| <i>To be specified:</i> |   |                              |
|-------------------------|---|------------------------------|
| Parameter               | Range ( <i>Default</i> )  | Label                        |
| <b>INS.FILT1.NAME</b>   | SIC PAH1 ARIII SIV_1 SIV SIV_2 PAH2 PAH2_2 NEII_1 NEII NEII_2 Q1 Q2 Q3 ( <i>NODEFAULT</i> ) | Imager Filter                |
| <b>INS.PFOV</b>         | 0.045 0.076 ( <i>0.076</i> )  | Imager pixel scale           |
| <b>SEQ.CHOPNOD.DIR</b>  | PARALLEL PERPENDICULAR ( <i>PERPENDICULAR</i> )   | Relative Chop/Nod Direction  |
| <b>SEQ.JITTER.WIDTH</b> | 0..10 ( <i>0</i> )  | Random Jitter Width (arcsec) |
| <b>SEQ.TIME</b>         | 30..3600 ( <i>NODEFAULT</i> )   | Total integration time (sec) |
| <b>SEQ.DIT.ALGO</b>     | AUTO, GOOD-WEATHER, BRIGHT-SOURCE ( <i>NODEFAULT</i> )                                      | DIT determination algorithm  |
| <b>TEL.CHOP.THROW</b>   | 8..30 ( <i>8</i> )  | Chopping Amplitude (arcsec)  |

**VISIR\_spec\_cal\_LRAutoChopNod.tsf**

| <i>To be specified:</i> |  |                                   |
|-------------------------|--|-----------------------------------|
| Parameter               | Range ( <i>Default</i> )                               | Label                             |
| <b>INS.GRAT1.WLEN</b>   | 10.5 ( <i>NODEFAULT</i> )                              | Spectrometer Wavelength (microns) |
| <b>SEQ.CHOPNOD.DIR</b>  | PARALLEL PERPENDICULAR ( <i>PARALLEL</i> )             | Relative Chop/Nod Direction       |
| <b>SEQ.JITTER.WIDTH</b> | 0..10 ( <i>0</i> )                                     | Random Jitter Width (arcsec)      |
| <b>SEQ.TIME</b>         | 30..3600 ( <i>NODEFAULT</i> )                          | Total integration time (sec)      |
| <b>SEQ.DIT.ALGO</b>     | AUTO, GOOD-WEATHER, BRIGHT-SOURCE ( <i>NODEFAULT</i> ) | DIT determination algorithm       |
| <b>TEL.CHOP.THROW</b>   | 8..30 ( <i>8</i> )                                     | Chopping Amplitude (arcsec)       |



**VISIR\_spec\_cal\_MRAutoChopNod.tsf**

*To be specified:*

| Parameter               | Range (Default)                               | Label                             |
|-------------------------|---|-----------------------------------|
| <b>INS.GRAT1.WLEN</b>   | 7.5..28.08 (NODEFAULT)                        | Spectrometer Wavelength (microns) |
| <b>SEQ.CHOPNOD.DIR</b>  | PARALLEL PERPENDICULAR (PARALLEL)             | Relative Chop/Nod Direction       |
| <b>SEQ.JITTER.WIDTH</b> | 0..10 (0)                                     | Random Jitter Width (arcsec)      |
| <b>SEQ.TIME</b>         | 30..3600 (NODEFAULT)                          | Total integration time (sec)      |
| <b>SEQ.DIT.ALGO</b>     | AUTO, GOOD-WEATHER, BRIGHT-SOURCE (NODEFAULT) | DIT determination algorithm       |
| <b>TEL.CHOP.THROW</b>   | 8..30 (8)                                     | Chopping Amplitude (arcsec)       |

**VISIR\_spec\_cal\_HRAutoChopNod.tsf**

*To be specified:*

| Parameter               | Range (Default)                               | Label                             |
|-------------------------|---|-----------------------------------|
| <b>INS.FILT2.NAME</b>   | NEII_2 H2S_1 H2S_4 (NEII_2)                   | Spectrometer Filter               |
| <b>INS.GRAT1.WLEN</b>   | 7.80..19.18 (12.810)                          | Spectrometer Wavelength (microns) |
| <b>SEQ.CHOPNOD.DIR</b>  | PARALLEL PERPENDICULAR (PARALLEL)             | Relative Chop/Nod Direction       |
| <b>SEQ.JITTER.WIDTH</b> | 0..10 (0)                                     | Random Jitter Width (arcsec)      |
| <b>SEQ.TIME</b>         | 30..3600 (NODEFAULT)                          | Total integration time (sec)      |
| <b>SEQ.DIT.ALGO</b>     | AUTO, GOOD-WEATHER, BRIGHT-SOURCE (NODEFAULT) | DIT determination algorithm       |
| <b>TEL.CHOP.THROW</b>   | 8..30 (8)                                     | Chopping Amplitude (arcsec)       |

**VISIR\_spec\_cal\_HRXAutoChopNod.tsf**

*To be specified:*

| Parameter               | Range (Default)                               | Label                             |
|-------------------------|---|-----------------------------------|
| <b>INS.GRAT1.WLEN</b>   | 7.60..28.08 (NODEFAULT)                       | Spectrometer Wavelength (microns) |
| <b>SEQ.CHOPNOD.DIR</b>  | PARALLEL PERPENDICULAR (PARALLEL)             | Relative Chop/Nod Direction       |
| <b>SEQ.JITTER.WIDTH</b> | 0..10 (0)                                     | Random Jitter Width (arcsec)      |
| <b>SEQ.TIME</b>         | 30..3600 (NODEFAULT)                          | Total integration time (sec)      |
| <b>SEQ.DIT.ALGO</b>     | AUTO, GOOD-WEATHER, BRIGHT-SOURCE (NODEFAULT) | DIT determination algorithm       |
| <b>TEL.CHOP.THROW</b>   | 8..30 (8)                                     | Chopping Amplitude (arcsec)       |

## 10 Appendix: Filter transmission curves

The filter transmission has been measured using a Fourier Transform Spectrometer, at a temperature of 35 K for filters manufactured by the company READING. Their absolute transmission curves are displayed in Fig. 19. The other filters, manufactured by OCLI, have been measured using the WCU and wavelength scans with the monochromator. Note that for these filters, the transmission curves are normalized to 1, see Fig. 19.

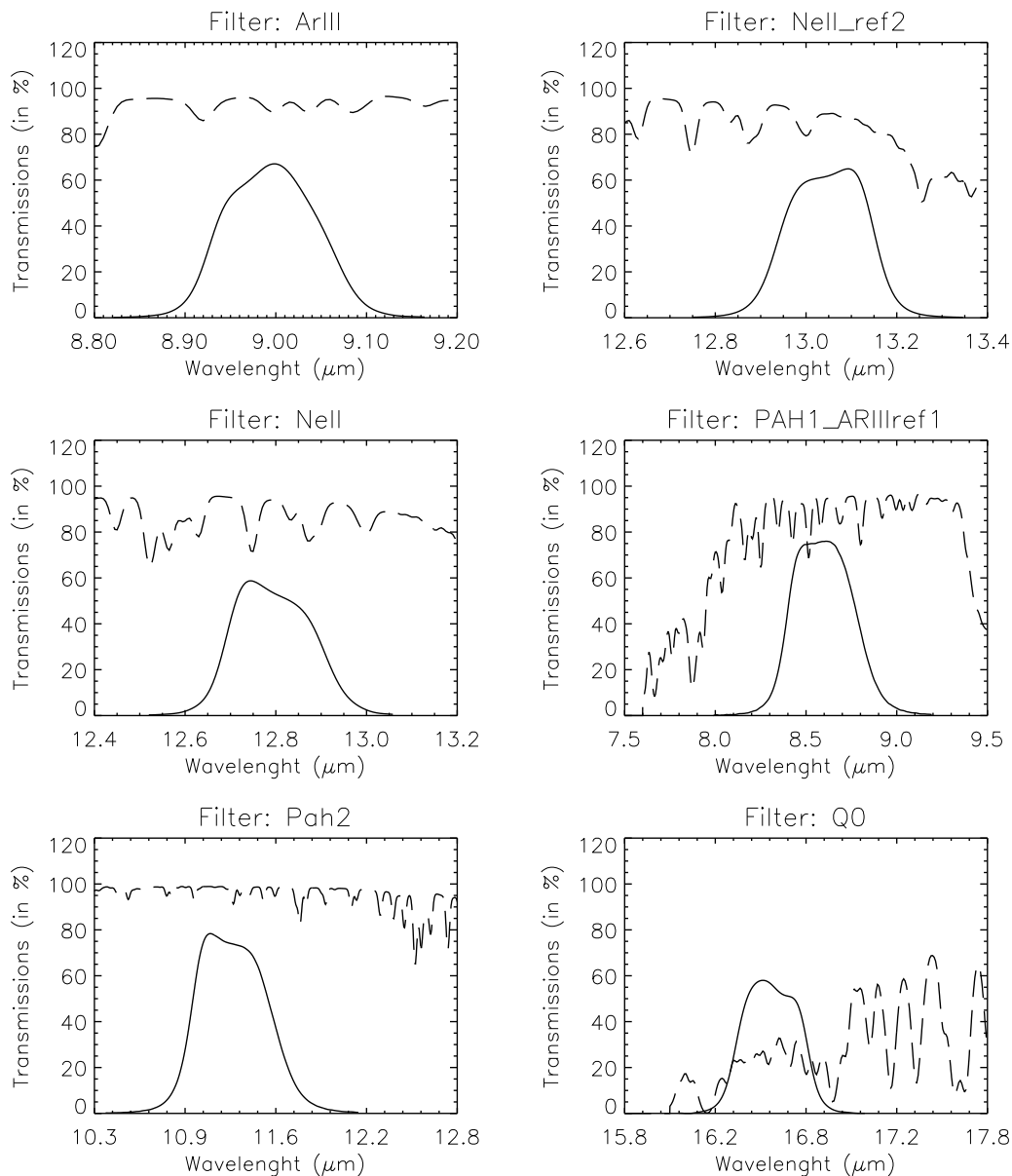


Figure 19: Transmission curves of VISIR imager filters, manufactured by READING. Overplotted (dashed) is the atmospheric transmission at low resolution. The absolute transmission values are given, expressed in percent.

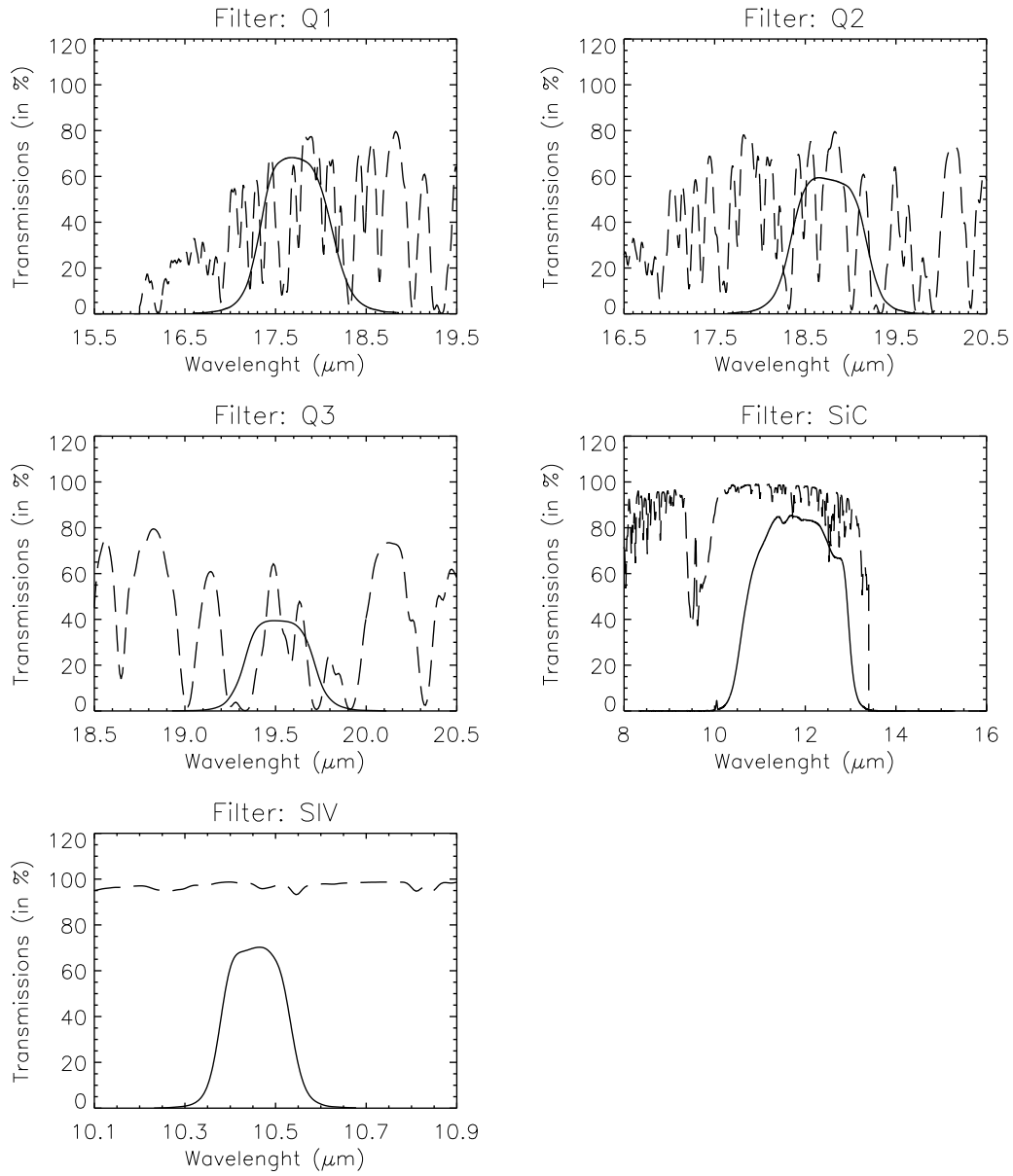


Figure 18: – continued.

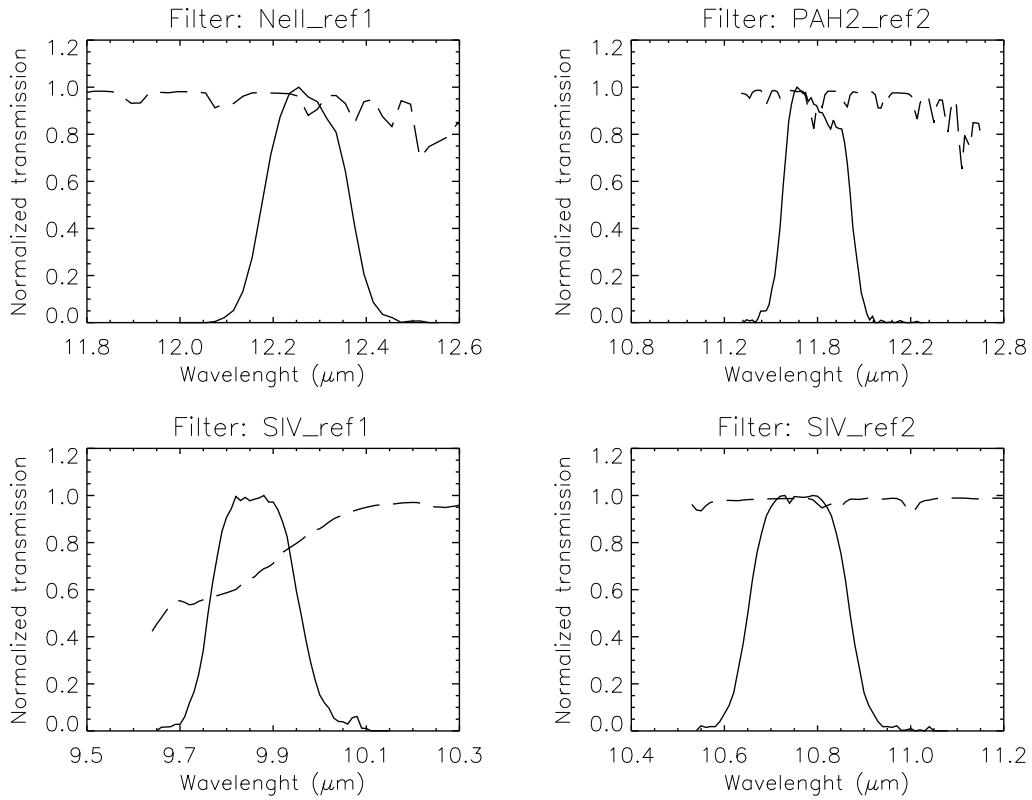


Figure 19: Transmission curves of VISIR imager filters, manufactured by OCLI. Overplotted (dashed) is the atmospheric transmission at low resolution. Only relative transmissions have been determined; their values are normalized so that their peak transmission is equal to 1.

## 11 Appendix: Observed sensitivities in various spectroscopic settings

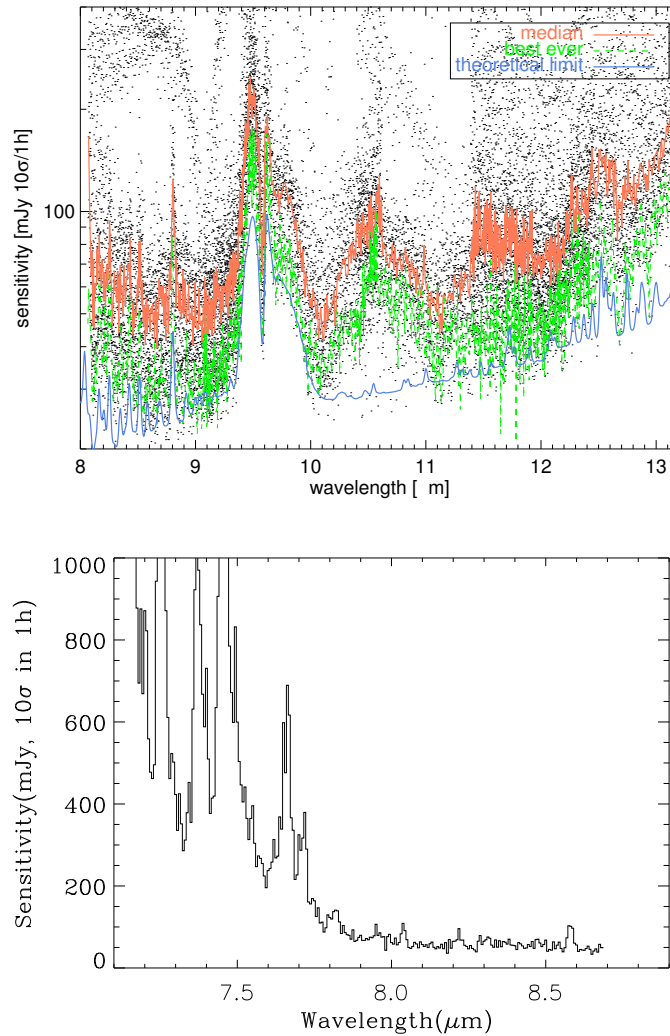


Figure 20: **Measured on the old DRS detector.** Sensitivity as a function of wavelength for low resolution mode. *Top*: Four offered settings of the N-band low-resolution are stitched together. Atmospheric molecular absorption, e.g. at  $9.55$ ,  $11.8$  and  $12.5 \mu\text{m}$ , is evident. Note the detector feature at  $8.8 \mu\text{m}$ . Dots indicate individual observations, full lines represent median and the dashed line the best sensitivities. Theoretical model curves correspond to BLIP. *Bottom*: Sensitivity measured in the bluer setting, centered at  $8.1 \mu\text{m}$ .

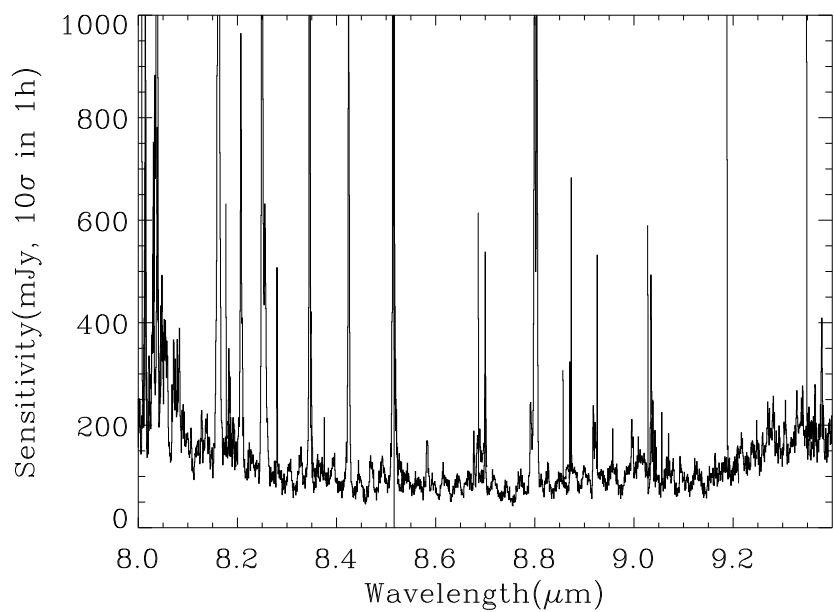
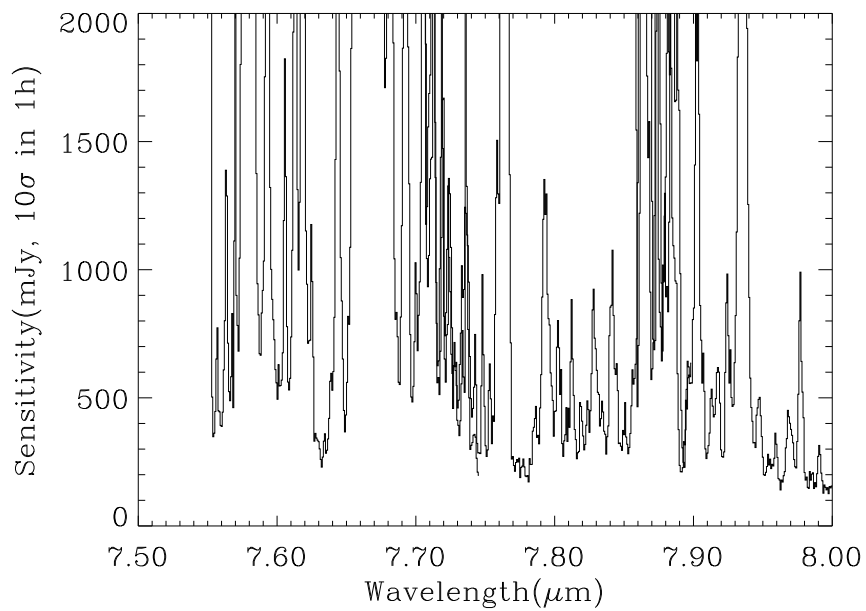


Figure 21: **Measured on the old DRS detector.** Observed sensitivity as a function of wavelength for different settings in the medium resolution mode obtained in very good weather conditions: (I) for  $7.5\mu\text{m} < \lambda < 9.4\mu\text{m}$  . Offered sensitivity is typically a factor of 2 larger.

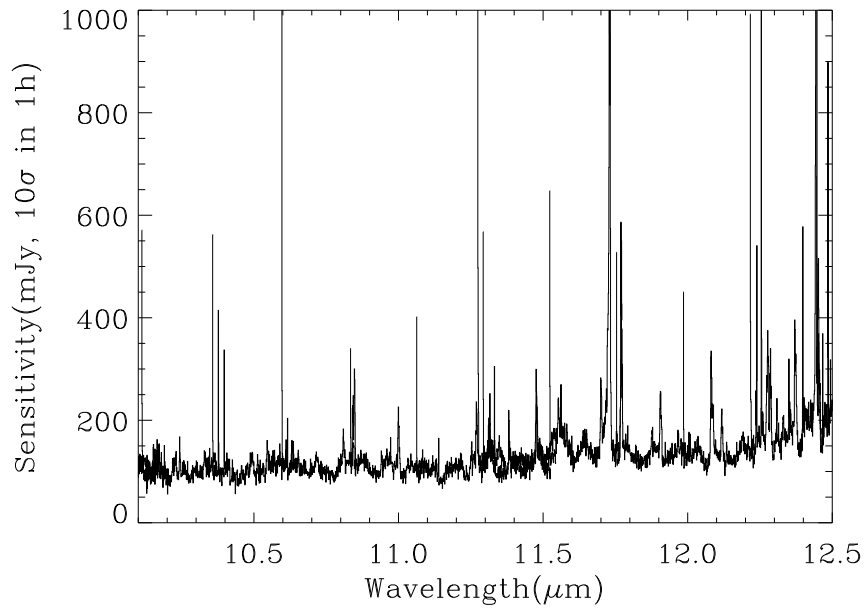


Figure 22: **Measured on the old DRS detector.** Observed sensitivity as a function of wavelength for different settings in the medium resolution mode obtained in very good weather conditions: (II) for  $10.1\mu\text{m} < \lambda < 12.5\mu\text{m}$  . Offered sensitivity is typically a factor of 2 larger.

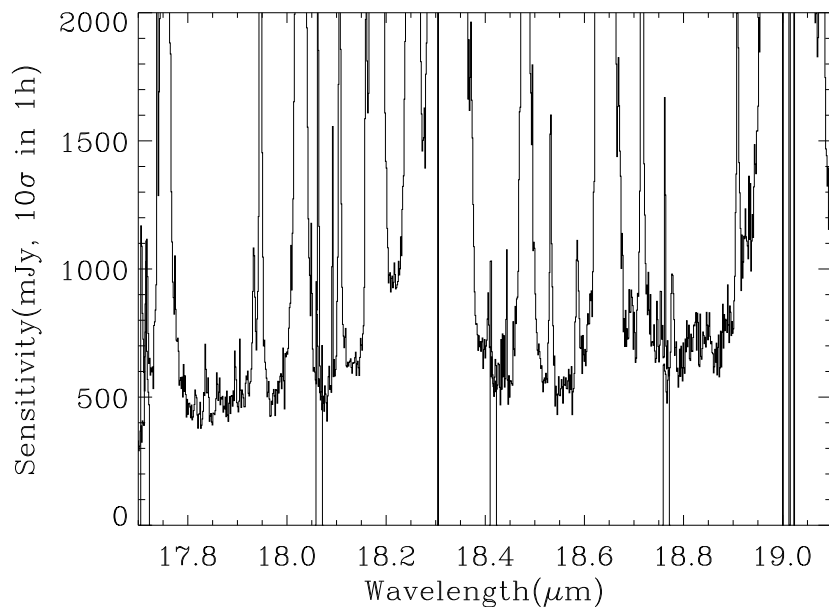


Figure 23: **Measured on the old DRS detector.** Observed sensitivity as a function of wavelength for different settings in the medium resolution mode obtained in very good weather conditions: (III) for  $17.7\mu\text{m} < \lambda < 19.1\mu\text{m}$  . Offered sensitivity is typically a factor of 2 larger.

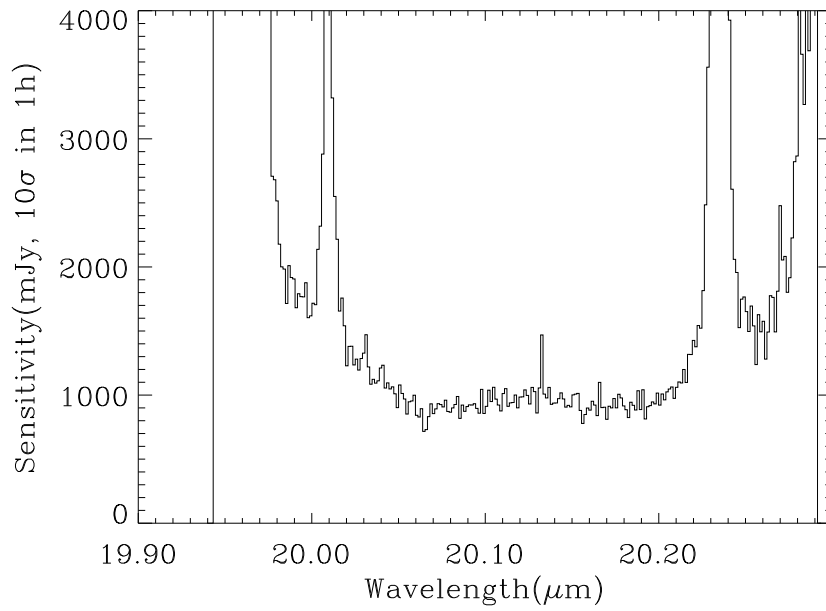


Figure 24: **Measured on the old DRS detector.** Observed sensitivity as a function of wavelength for different settings in the medium resolution mode obtained in very good weather conditions: (IV) for  $19.9\mu\text{m} < \lambda < 20.3\mu\text{m}$  . Offered sensitivity is typically a factor of 2 larger.

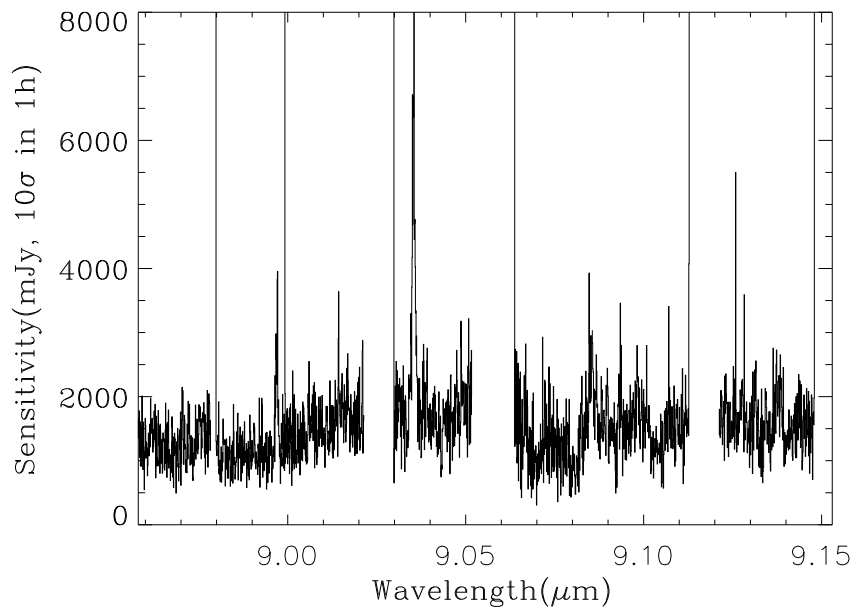


Figure 25: **Measured on the old DRS detector.** Observed sensitivity as a function of wavelength for high resolution mode. Offered sensitivity is typically a factor of 2 larger.



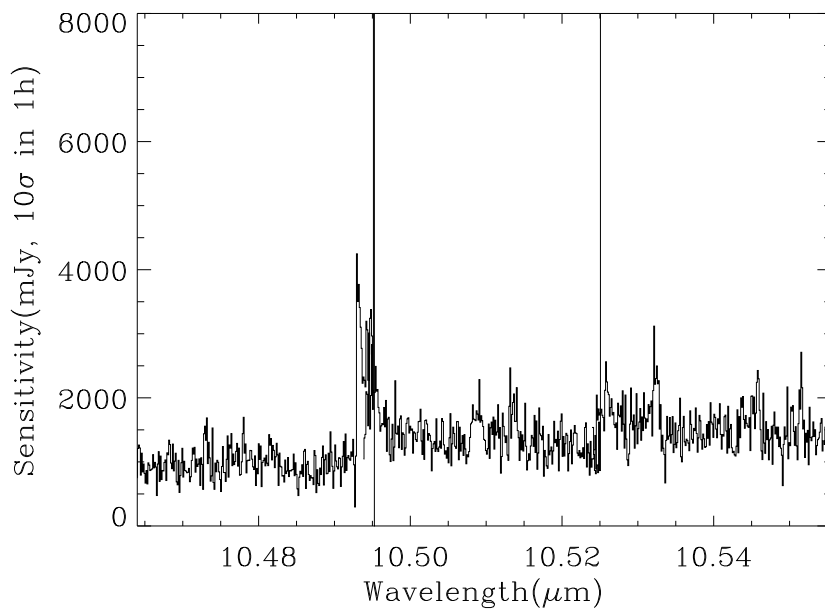


Figure 26: **Measured on the old DRS detector.** Observed sensitivity as a function of wavelength for high resolution mode. Offered sensitivity is typically a factor of 2 larger.

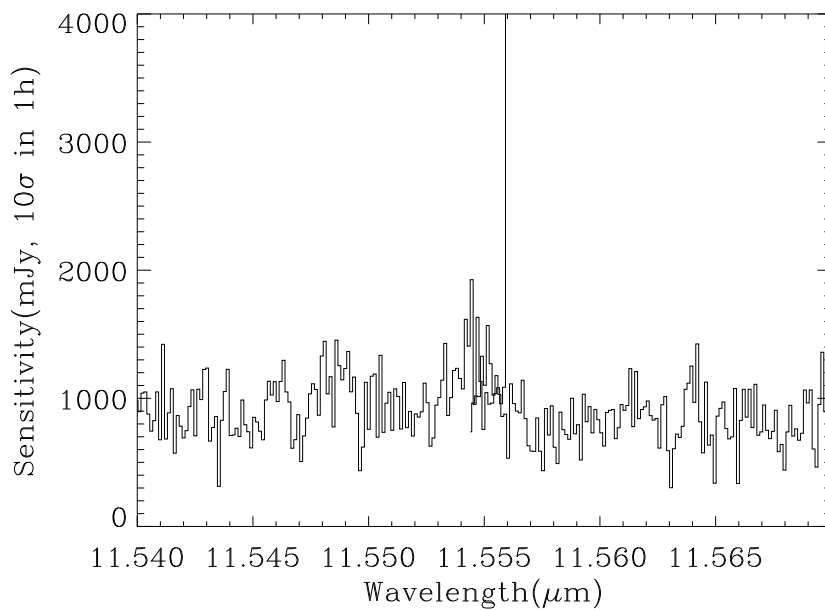


Figure 27: **Measured on the old DRS detector.** Observed sensitivity as a function of wavelength for high resolution mode. Offered sensitivity is typically a factor of 2 larger.

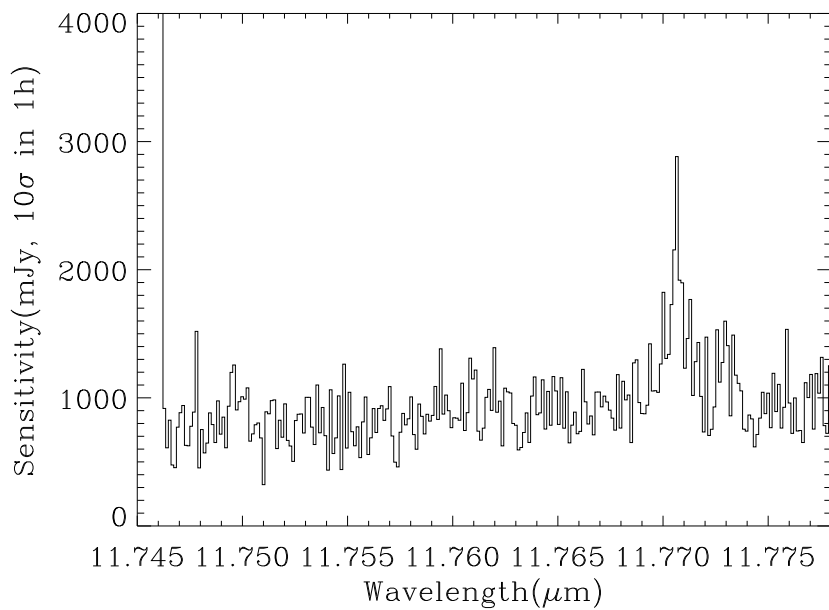


Figure 28: **Measured on the old DRS detector.** Observed sensitivity as a function of wavelength for high resolution mode. Offered sensitivity is typically a factor of 2 larger.

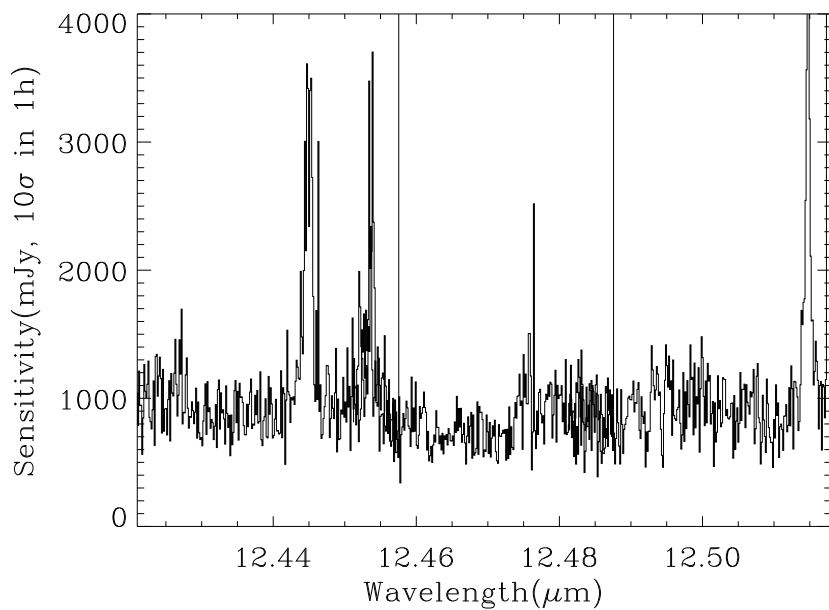


Figure 29: **Measured on the old DRS detector.** Observed sensitivity as a function of wavelength for high resolution mode. Offered sensitivity is typically a factor of 2 larger.

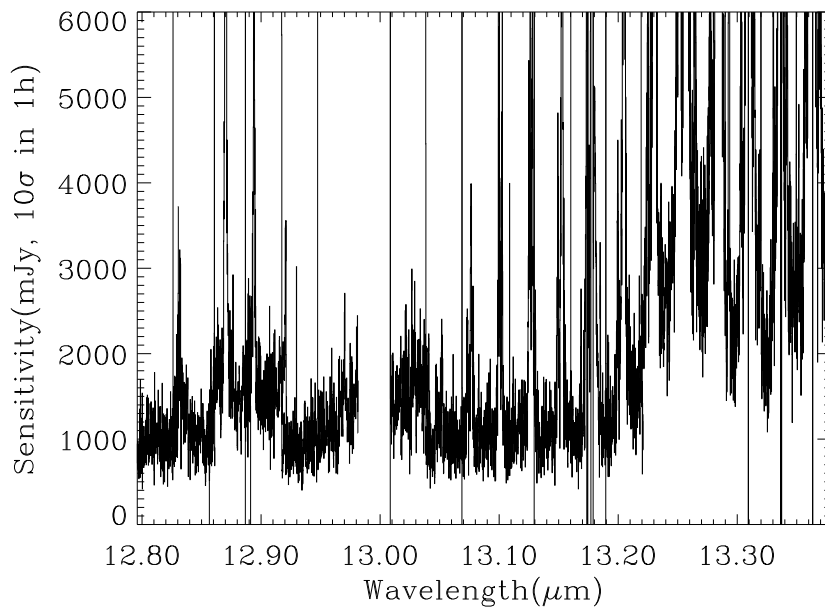
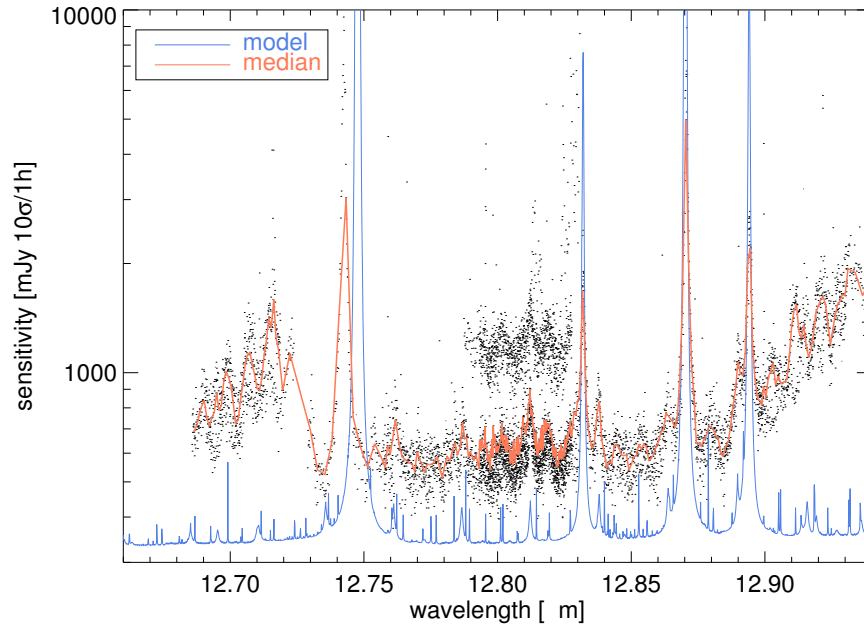


Figure 30: **Measured on the old DRS detector.** Observed sensitivity as a function of wavelength for high resolution mode. *Top:* Observed sensitivities obtained on various nights, compared with the theoretical model curves, corresponding to BLIP. *Bottom:* Sensitivities over an extended region encompassing the observed wavelength of [NeII] up to  $z \approx 0.038$ .

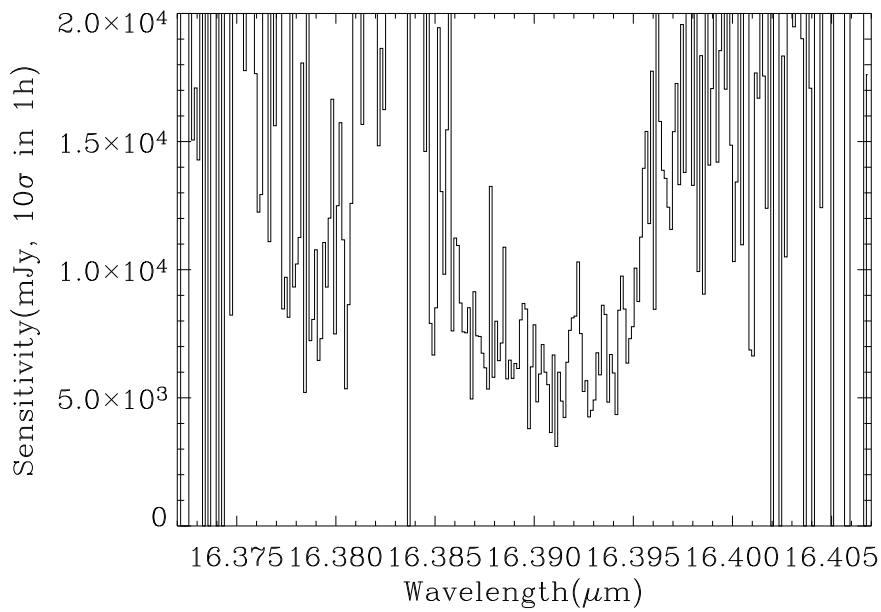


Figure 31: **Measured on the old DRS detector.** Observed sensitivity as a function of wavelength for high resolution mode. Offered sensitivity is typically a factor of 2 larger.

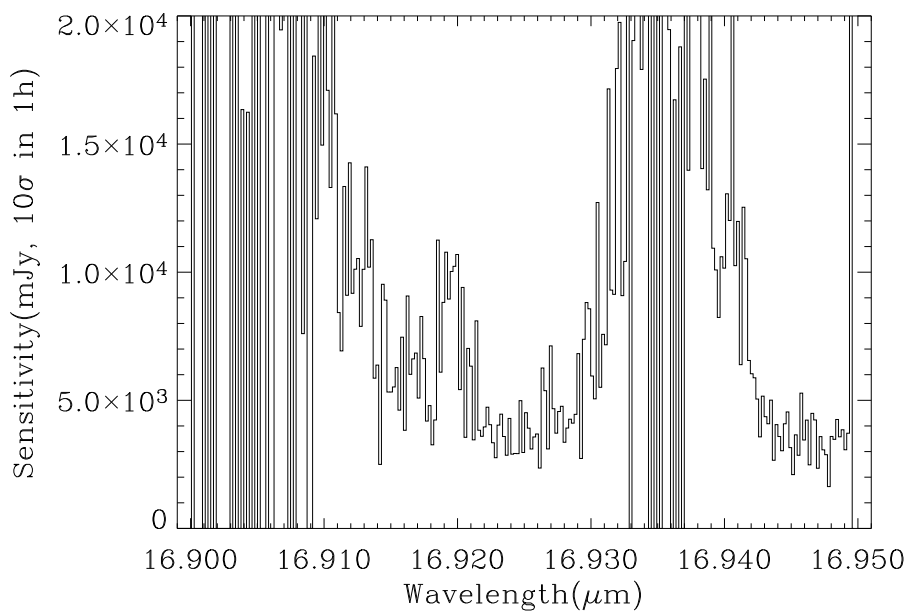


Figure 32: **Measured on the old DRS detector.** Observed sensitivity as a function of wavelength for high resolution mode. Offered sensitivity is typically a factor of 2 larger.

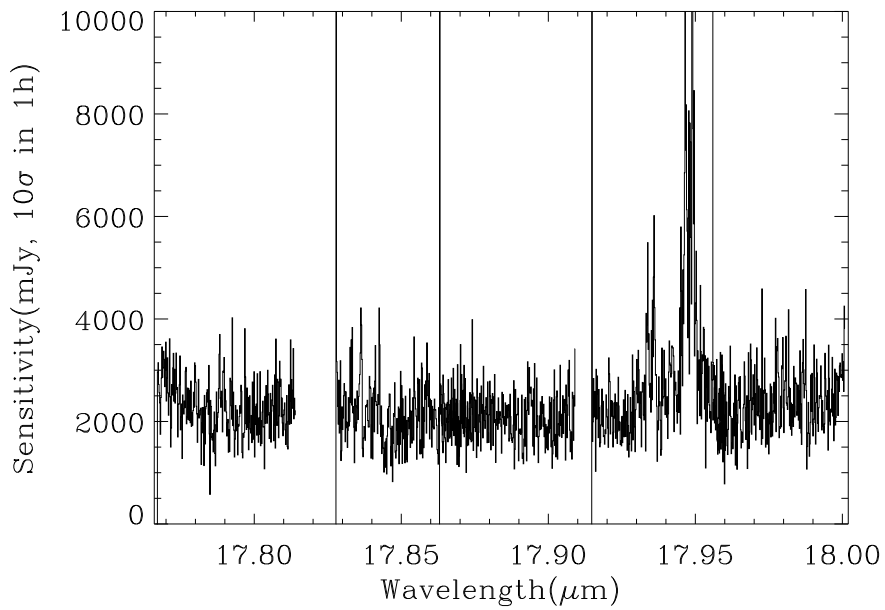


Figure 33: **Measured on the old DRS detector.** Observed sensitivity as a function of wavelength for high resolution mode. Offered sensitivity is typically a factor of 2 larger.

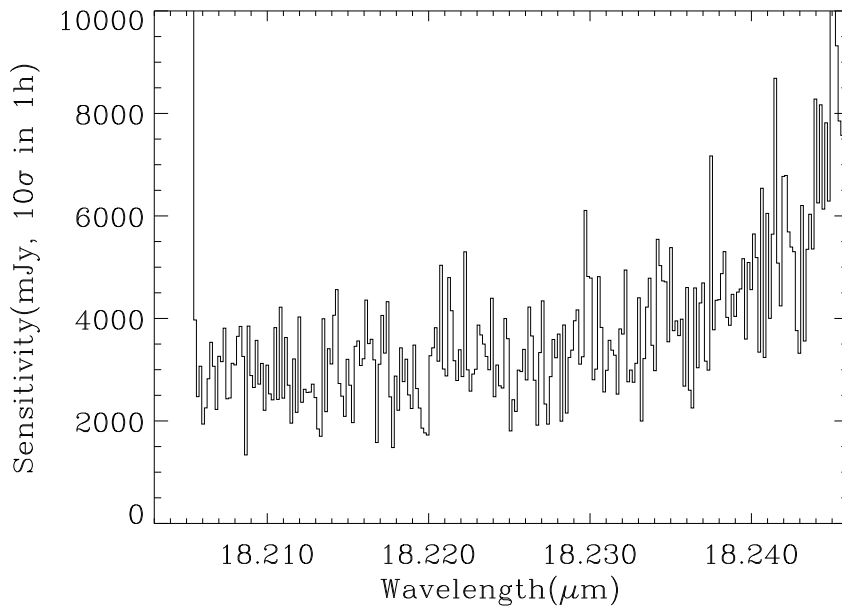


Figure 34: **Measured on the old DRS detector.** Observed sensitivity as a function of wavelength for high resolution mode. Offered sensitivity is typically a factor of 2 larger.

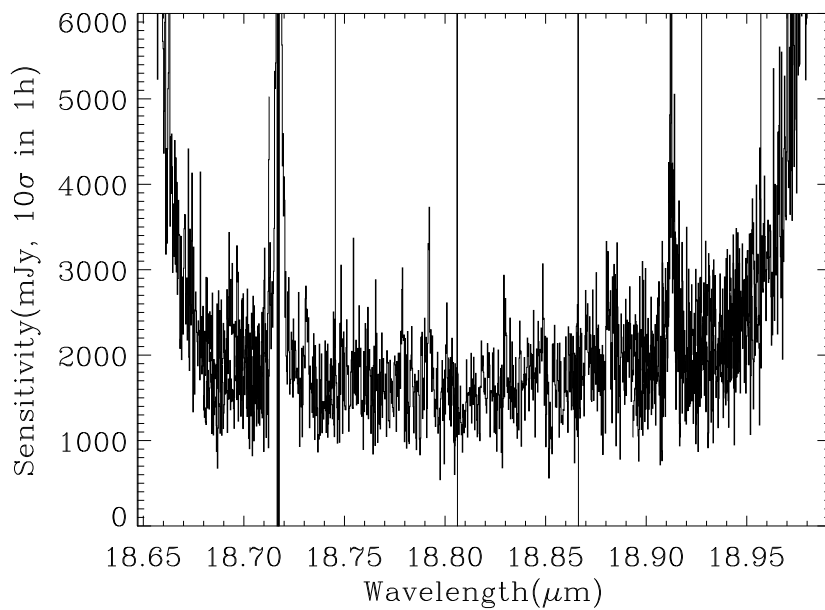


Figure 35: **Measured on the old DRS detector.** Observed sensitivity as a function of wavelength for high resolution mode. Offered sensitivity is typically a factor of 2 larger.

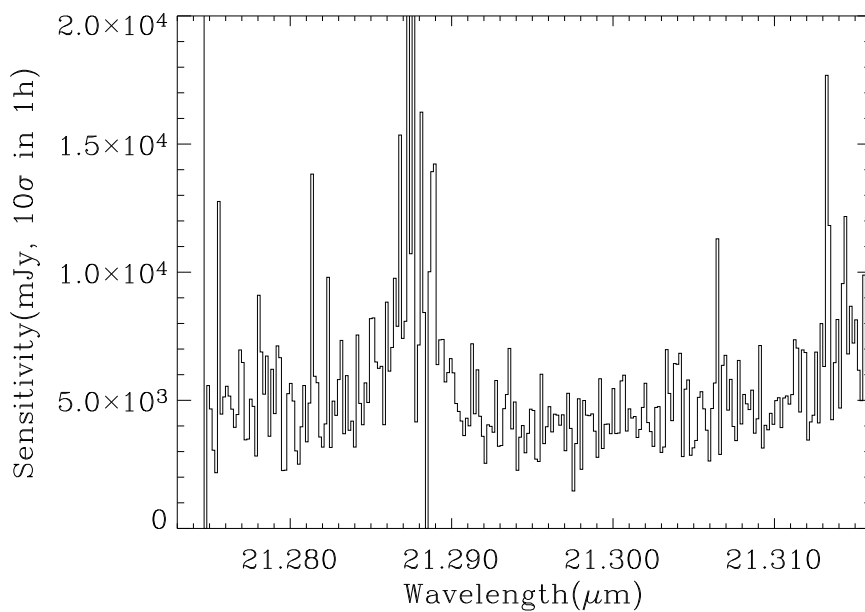


Figure 36: **Measured on the old DRS detector.** Observed sensitivity as a function of wavelength for high resolution mode. Offered sensitivity is typically a factor of 2 larger.